Supplemental Methods

Analysis of public data

We downloaded the raw small RNA sequence files (.bam files) from the Cancer Genomics Hub (CGHub) (1) with permission of the data access committee and extracted raw reads (FASTQ format) from BAM files of TCGA database using the "bamToFastq", a subcommand of the genome arithmetic toolset "BEDtools2" (v2.25.0). FASTQ files were analyzed with MINTmap (2) software for identification of tRFs and their abundance. We chose tRFs with RPM ≥ 0.1 and present in > 80% of total samples and by this definition, 368 tRFs in TCGA PAAD dataset were selected for further analysis. The correlations between the tRFs levels and survival time in patients with PDAC in TCGA database was estimated by Kaplan-Meier plot with log-rank test and univariate Cox proportional hazard regression analysis. *P*-values were adjusted by false discovery rate (FDR) and FDR < 0.25 was considered significant. We also analyzed the correlations between tRF-21 levels and survival time in patients with ESCA, COAD, LIHC, STAD, LUSC, LUAD, PRAD or BRCA in the TCGA database using the same methods as used for PDAC.

In silico analysis

The 3D structure of hnRNP L were predicted using I-TASSER (3) and *tRF-21* using SimRNAweb (4), respectively. The structure of hnRNP L-*tRF-21* complex was modeled with HDOCK (5) and visualized through PyMOL. We retrieved SRSF5 iCLIP-seq data from the GEO database (GSE113813) (6) for analyzing SRSF5 and tRNA binding sites. Adaptors and low-quality bases were trimmed by Cutadapt (v1.16) (7) and reads < 20 nucleotides were discarded. Reads were demultiplexed based on their experimental barcode using the pyBarcodeFilter.py script of the pyCRAC suite of tools (8). Sequence-based removal of PCR duplicates was then performed with the pyFastqDuplicateRemover.py script (8). Reads were then mapped to the human genome (hg19) with BWA (v0.7.15) (9) using the parameter 'bwa aln -n 0.06 -q 20'. Next, we detected crosslinking-induced mutation sites (CIMSs) and crosslinking-induced truncation sites (CITSs) using

the CLIP Tool Kit (CTK) (10) as previously described (11). For CIMS analysis, the coverage of unique tags (k) and mutations (m) were determined by the CIMS.pl script of the CLIP Tool Kit. Only mutation positions with m/k ≥ 50% were identified as CIMS. CITS sites were identified with the CITS.pl script, and sites with $P \leq 0.05$ were defined as CITS. Sequence alignment indicated binding of SRSF5 to $tRNA^{GlyGCC}$, which was visualized by Integrative Genomics Viewer (IGV) (12).

Cell lines and cell culture

Capan-2, SW1990 and 293T cell lines were purchased from the Cell Bank of the Type Culture Collection of Chinese Academy of Sciences, Shanghai Institute of Biochemistry and Cell Biology. All cell lines were certified by DNA fingerprinting analysis using short-tandem repeat (STR) markers. In addition, all cells were tested for mycoplasma and were uninfected. Capan-2, SW1990 and 293T cells were cultured in DMEM with 10% FBS in an atmosphere of 5% CO_2 and 99% relative humidity at 37°C.

Transient transfection of *tRF-21* mimics, siRNAs and plasmids

tRF-21 mimics and siRNAs (**Supplementary Table 6**) were synthesized by GenePharma. cDNAs encoding SRSF5 and KLF4 were individually subcloned into the pcDNA3.1 vector (Umine Biotechnology) and the resultant vectors were named pcDNA3.1-SRSF5 and pcDNA3.1-KLF4, respectively. Blank pcDNA3.1 vector was served as control. Transfection with mimics (50 nM), plasmids (1 ng/ml) or siRNAs (50 nM) was performed with Lipofectamine 2000 (Life Technologies).

Northern blot assays

Total RNA (15 μg) from PDAC cells was subject to 15% denaturing polyacrylamide gel electrophoresis and then transferred to Biodyne Nylon Membrane (Pall). After pre-hybridization for 30 min, membrane was hybridized overnight at 68 °C in DIG Easy Hybrid buffer containing the denatured *tRF-21* probe labeled with digoxigenin from BersinBio (**Supplementary Table 7**). After washing, membrane was incubated with anti-digoxigenin-AP and signal on the membrane was detected using an Odyssey infrared scanner (Li-Cor, Lincoln).

qRT-PCR and four-leaf clover qRT-PCR analysis

Total RNA extracted from cell lines and pancreatic tissue specimens with TRIzol reagent (Invitrogen) was reverse transcribed with random primers or specific tRF stem-loop RT primers. Relative RNA level was measured by quantitative real-time PCR (qRT-PCR) on a Light Cycler 480 II (Roche Diagnostics) using the SYBR Green method. *U6* RNA was used as an internal control for quantification of tRFs. Three biological replicates were set up for each experiment. The relative expression level was determined with the $2^{-\Delta Ct}$ method. The primer sequences are shown in **Supplemental Table 7**. Determination of $tRNA^{GlyGCC}$ was accomplished with four-leaf clover qRT-PCR (13). Briefly, total RNA was first subjected to deacylation treatment and then specifically hybridized with DNA/RNA hybrid SL-adaptor (200 pmol, Integrated DNA Technologies), followed by ligation with T4 RNA ligase 2 (NEB) to form a four-leaf clover structure. Reverse transcription was achieved with the SuperScript™ III Reverse Transcriptase (Life Technologies) and specific RT primers and resultant cDNA was subject to qPCR. 5S *rRNA* was quantified as an internal control. The sequences of primer pairs, SL-adapter and the TaqMan probe for $tRNA^{GlyGCC}$ and *5S rRNA* detection are shown in **Supplementary Table 7**.

Measuring absolute *tRF-21* copy number in cell

An accurate *tRF-21* copy number per cell was determined by qRT-PCR as described (14, 15). Briefly, synthetic *tRF-21* at 4 different dilutions was applied to formulate a standard curve and each Ct value represented an exact *tRF-21* level. The exact *tRF-21* copy number per cell was then calculated taking the *tRF-21* molecular weight and cell count into account.

Subcellular fractionating

Cytosolic and nuclear fractions of Capan-2 and SW1990 cells were prepared and collected according to the instructions of the PARIS™ Kit Protein and RNA Isolation System (AM1921, Thermo Fisher). The levels of *tRF-21* and interest proteins were determined in each fraction.

Lentivirus production, transduction and plasmids construction

Lentivirus-mediated *tRF-21* expression or silencing was achieved by the documented method (16) with some modifications. Briefly, for expressing, the synthesized *tRF-21* sequence was inserted into pLKD-CMV-mcherry-2A-Neo-U6-shRNA vector containing the miR-30 backbone (OBiO Technology). For silencing, the *tRF-21* antisense sequence was inserted into the lentiviral vector pLKD-CMV-mcherry-2A-Neo-U6-shRNA. The plasmid and its insertion sequences were authentic by DNA sequencing. These vectors and a lentiviral vector packaging system (OBiO Technology) were then cotransfected into 293T cells using Lipofectamine 2000. The resultant lentiviruses were designated *tRF-21* expression or *tRF-21* silencing, respectively. Capan-2 and SW1990 cells were infected with these lentiviruses in the presence of polybrene (Sigma-Aldrich) and selected by puromycin. The alternations of *tRF-21* levels in cells were detected by qRT-PCR.

For constructing FLAG-tagged hnRNP L expression vectors, synthesized full-length, truncated or mutated *HNRNPL* cDNA was respectively subcloned into the pcDNA3.1-3× FLAG vector (OBiO Technology). The same method was also used for constructing FLAG-tagged SRSF5 expression vector. For constructing HA-tagged DDX17 expression vector, synthesized full-length or truncated *DDX17* cDNA was subcloned into the pcDNA3.1-HA vector (OBiO Technology).

Analysis of cell malignant phenotypes

Cell viability was measured with the CCK-8 kit (Dojindo) and colony formation ability was determined by counting the methanol-fixed and crystal violet-stained colonies. Apoptosis was analyzed by flow cytometry (Beckman Coulter) with the Annexin V–FITC Apoptosis Detection kit (Invitrogen). Cell invasion ability was measured in Millicell chamber with 8-μm pores coated with 30 μg of Matrigel (BD Biosciences). Briefly, cells (1×10^5) in serum-free medium were added to the upper chamber with pre-coated filter and medium containing fetal bovine serum was added to the lower chamber. After incubation for 20 h at 37°C and 5% CO_2, cells migrated through the filters were fixed with methanol, dyed with crystal violet and photographed. Cells in three random fields were counted. Migration ability was tested using the same method but the inserts were not coated

with Matrigel.

RNA pulldown assays

RNA pulldown was performed with the Pierce™ Magnetic RNA-Protein Pull-Down Kit (20164, Thermo Fisher). Briefly, biotinylated non-targeting oligo, *tRF-21* or its antisense (GenePharma) was incubated with protein extracts from cells. Streptavidin beads were then added, and total proteins associated with *tRF-21* or its antisense was subjected to mass spectrometry or Western blot analysis. Similarly, biotinylated *tRF-21* was incubated with protein extracts from cells transfected with full-length, truncated or mutated hnRNP L; biotinylated $tRNA^{GlyGCC}$ generated by in vitro transcription was incubated with protein extracts from cells transfected with full-length or truncated SRSF5. Streptavidin beads were then added, and total proteins associated with *tRF-21* or $tRNA^{GlyGCC}$ were subjected to Western blot analysis.

Protein immunoprecipitation

Protein immunoprecipitation was performed with the Pierce™ Crosslink Magnetic IP/Co-IP Kit (88805, Thermo Fisher). Cells were lysed in lysis buffer supplemented with the Protease/Phosphatase Inhibitor Cocktail (Pierce) for 30 min on ice. Lysate was incubated with the indicated antibodies crosslinked to Protein A/G magnetic beads for 2 hours at room temperature. After washing 3 times with immunoprecipitation lysis buffer, bound antigens were then eluted.

Mass spectrum analysis

Eluate containing proteins associated with *tRF-21* from RNA pulldown or proteins binding p-Ser52-hnRNP L from protein immunoprecipitation was firstly digested into peptides and then subjected to mass spectrum analysis with TripleTOF® 6600 mass spectrometer and Eksigent NanoLC 2D Plus system (AB SCIEX). ProteinPilot 5.0 software (AB SCIEX) was used for analysis and proteins were ranked by the exponentially modified protein abundance index (emPAI) (**Supplementary Tables 2 and 3**).

Cell lysis and Western blot analysis

PDAC cells transfected with full-length or truncated HA-tagged DDX17 or FLAG-tagged full-length, truncated or mutated hnRNP L were lysed with 1× RIPA buffer supplemented with the Protease/Phosphatase Inhibitor Cocktail (Pierce). Lysate was centrifuged and the supernatant was collected. Protein extract was then separated on SDS-PAGE and transferred to PVDF membrane (Millipore). The membrane was incubated overnight at 4°C with specific primary antibody against the interest protein (**Supplementary Table 8**) and visualized with a Phototope Horseradish Peroxidase Western Blot Detection kit (WBKLS0100, Millipore). Antibodies against p-Ser52-hnRNP L and Caspase 9a/b were customized by GenScript. A peptide containing phosphorylated Ser52 of hnRNP L or the shared sequence of Caspase 9a and Caspase 9b was synthesized and injected into New Zealand rabbits. After the 3rd immunization, antiserum was tested and further purified for the customized polyclonal antibody. All uncropped immunoblot images in this study were provided in **Supplementary Figure 17**.

RNA immunoprecipitation assays

RNA immunoprecipitation (RIP) assays were performed using the Magna RIP RNA-Binding Protein Immunoprecipitation kit (17-700, Millipore). Antibody against hnRNP L, SRSF5, RBM4, MBNL1 or FLAG is shown in Supplemental Table 6**.** The co-precipitated RNAs were detected by qRT-PCR or four-leaf clover-PCR.

Chromatin immunoprecipitation assays

Chromatin immunoprecipitation (ChIP) assays were performed using the EZ-Magna ChIP^{TM} A/G Kit (17-10086, Millipore). Briefly, cells were cross-linked with 1% formaldehyde; lysed and sonicated on ice to generate DNA fragments with an average length of 200–500 bp. Pre-cleared DNA was then immunoprecipitated with ChIP-grade KLF4 antibody. IgG was included as nonspecific control. DNA was eluted, purified and subject to qRT-PCR.

Immunohistochemical staining

Ki67 and p-Ser52-hnRNP L protein levels in tissue slides were determined by

immunohistochemical staining with Ki67 antibody (1:50, ZSGB-BIO, ZA-0502) or p-Ser52-hnRNP L antibody (1:50, GenScript). Apoptosis level was determined by terminal deoxynucleotidyl transferase-mediated dUTP nick end labeling (TUNEL) using Klenow FragEL^{TM} DNA Fragmentation Detection Kit (EMD Biosciences). Ki67 and TUNEL indexes were evaluated by percentage of positive staining cells. We applied immune reactive score (IRS) to determine p-Ser52-hnRNP L level. The intensity of p-Ser52-hnRNP L labeling score was estimated as negative (0), weak (1), moderate (2) and strong (3). The extent of staining, defined as the percentage of positive staining cells, was scored as 1 (≤ 25%), 2 (26%–50%), 3 (51%–75%) and 4 (> 75%). The total IRS was obtained by multiplying the score of intensity and extent.

RNA FISH and immunofluorescence

Fluorescent in situ hybridization (FISH) was performed with Ribo™ Fluorescent In Situ Hybridization Kit (RiboBio). Briefly, fixed and permeabilized PDAC cells were hybridized with *tRF-21* probes (RiboBio) overnight in a humidified chamber at 37°C in the dark and the images were obtained with Olympus FV1000 confocal microscope (Olympus). The signals were detected by using 4',6-diamidino-2-phenylindole and Cy3 channels. Cell nuclei were counterstained with DAPI. Antibodies against p-Ser52-hnRNP L (1:200, GenScript) and secondary antibody (1:500, A-21206, Invitrogen) were used for immunofluorescence staining. For immunofluorescent analysis, the tissue sections were incubated with p-Ser52-hnRNP L (1:500, GenScript) and DDX17 (1:250, Proteintech) followed by incubation with secondary antibodies (1:500, GB23303, Servicebio) according to the experiments design. The signals were detected by using FITC and Cy3 channels. Cell nuclei were counterstained with DAPI. Images were obtained with LSM880 confocal microscope (Zeiss).

Stress formation and cytokine treatment of PDAC cells

To form hypoxia, PDAC cells were incubated with DMEM containing 50 μM $CoCl_2$ (Sigma) for 24 h at 37°C (17, 18). To produce oxidative stress, PDAC cells were treated with 5 mM H_2O_2 for 4 h

(19). For nutrition starvation, PDAC cells were washed and then complete medium were replaced with PBS for 30 min (18, 20).

PDAC cells were incubated with each cytokine dissolved in endotoxin-free water containing 0.5% BSA. Different cytokine concentrations and incubation times were used. For TNF-α (Novoprotein) were 10, 20 and 40 ng/ml for 12 h; for LIF (Novoprotein) were 0.5, 1.0 and 1.5 ng/ml for 15 min; for IL-10 (Novoprotein) were 10, 20 and 40 ng/ml for 48 h; for IL-6 (Sigma) were 50, 100 and 500 ng/ml for 1 h and for IL-1α (Sigma) were 1.0, 5.0 and 10 ng/ml for 1 h.

Reporter gene assays

Reporter gene assays were conducted as described (21). Briefly, the *SRSF5* promoter sequence (1 kb around the transcription start site) was cloned into the pGL4-promoter vector (Promega). PDAC cells were concurrently transfected with 400 ng of blank pGL4-promoter vector or vector containing *SRSF5* promoter, 4 ng of pRL-SV40 Renilla (Promega) luciferase reporter vector, 50 nM of siRNA targeting *KLF4* mRNA or scramble and 250 ng of pcDNA3.1 vector or vector containing *KLF4* cDNA and incubated with different concentrations of LIF or IL-6 for 48 h. The luciferase activities were determined by a Dual-Luciferase Reporter Assay System (Promega) and the relative Fluc/Rluc activity was calculated by normalizing the activity of firefly luciferase to that of Renilla luciferase.

References

1. Wilks C, et al. The Cancer Genomics Hub (CGHub): overcoming cancer through the power of torrential data. *Database (Oxford)*. 2014;2014:bau093.
2. Loher P, et al. MINTmap: fast and exhaustive profiling of nuclear and mitochondrial tRNA fragments from short RNA-seq data. *Sci Rep.* 2017;7:41184.
3. Yang J, Zhang Y. I-TASSER server: new development for protein structure and function predictions. *Nucleic Acids Res.* 2015;43(W1):W174–W181.
4. Magnus M, et al. SimRNAweb: a web server for RNA 3D structure modeling with optional restraints. *Nucleic Acids Res.* 2016;44(W1):W315–W319.

5. Yan Y, et al. HDOCK: a web server for protein-protein and protein-DNA/RNA docking based on a hybrid strategy. *Nucleic Acids Res.* 2017;45(W1):W365–W373.
6. Krchnakova Z, et al. Splicing of long non-coding RNAs primarily depends on polypyrimidine tract and 5' splice-site sequences due to weak interactions with SR proteins. *Nucleic Acids Res.* 2019;47(2):911–928.
7. Martin M. Cutadapt removes adapter sequences from high-throughput sequencing reads. *EMBnet J.* 2011;17(1):10–12.
8. Webb S, et al. PAR-CLIP data indicate that Nrd1-Nab3-dependent transcription termination regulates expression of hundreds of protein coding genes in yeast. *Genome Biol.* 2014;15(1):R8.
9. Li H, Durbin R. Fast and accurate short read alignment with Burrows-Wheeler transform. *Bioinformatics.* 2009;25(14):1754–1760.
10. Shah A, et al. CLIP Tool Kit (CTK): a flexible and robust pipeline to analyze CLIP sequencing data. *Bioinformatics.* 2017;33(4):566–567.
11. Weyn-Vanhentenryck SM, et al. HITS-CLIP and integrative modeling define the Rbfox splicing-regulatory network linked to brain development and autism. *Cell Rep.* 2014;6(6):1139–1152.
12. Robinson JT, et al. Integrative genomics viewer. *Nat Biotechnol.* 2011;29(1):24–26.
13. Honda S, et al. Four-leaf clover qRT-PCR: A convenient method for selective quantification of mature tRNA. *RNA Biol.* 2015;12(5):501–508.
14. Mai D, et al. PIWI-interacting RNA-54265 is oncogenic and a potential therapeutic target in colorectal adenocarcinoma. *Theranostics.* 2018;8(19):5213–5230.
15. Tan L, et al. PIWI-interacting RNA-36712 restrains breast cancer progression and chemoresistance by interaction with SEPW1 pseudogene SEPW1P RNA. *Mol Cancer.* 2019;18(1):9.
16. Scherr M, et al. Lentivirus-mediated antagomir expression for specific inhibition of miRNA function. *Nucleic Acids Res.* 2007;35(22):e149.
17. Wilson JL, et al. Endothelins induce CCR7 expression by breast tumor cells via endothelin receptor A and hypoxia-inducible factor-1. *Cancer Res*. 2006;66(24):11802–11807.
18. Fu H, et al. Stress induces tRNA cleavage by angiogenin in mammalian cells. *FEBS Lett*. 2009;583(2):437–442.
19. Thompson DM, et al. tRNA cleavage is a conserved response to oxidative stress in eukaryotes.

RNA. 2008;14(10):2095–2103.

20. Johannessen CM, et al. The NF1 tumor suppressor critically regulates TSC2 and mTOR. *Proc Natl Acad Sci USA*. 2005;102(24):8573–8578.
21. Zhang J, et al. Excessive miR-25-3p maturation via N(6)-methyladenosine stimulated by cigarette smoke promotes pancreatic cancer progression. *Nat Commun.* 2019;10(1):1858.
22. Dardenne E, et al. Splicing switch of an epigenetic regulator by RNA helicases promotes tumor-cell invasiveness. *Nat Struct Mol Biol.* 2012;19(11):1139–1146.
23. Shankarling G, Lynch KW. Living or dying by RNA processing: caspase expression in NSCLC. *J Clin Invest.* 2010;120(11):3798–3801.

Pan et al. Supplementary Figure 1

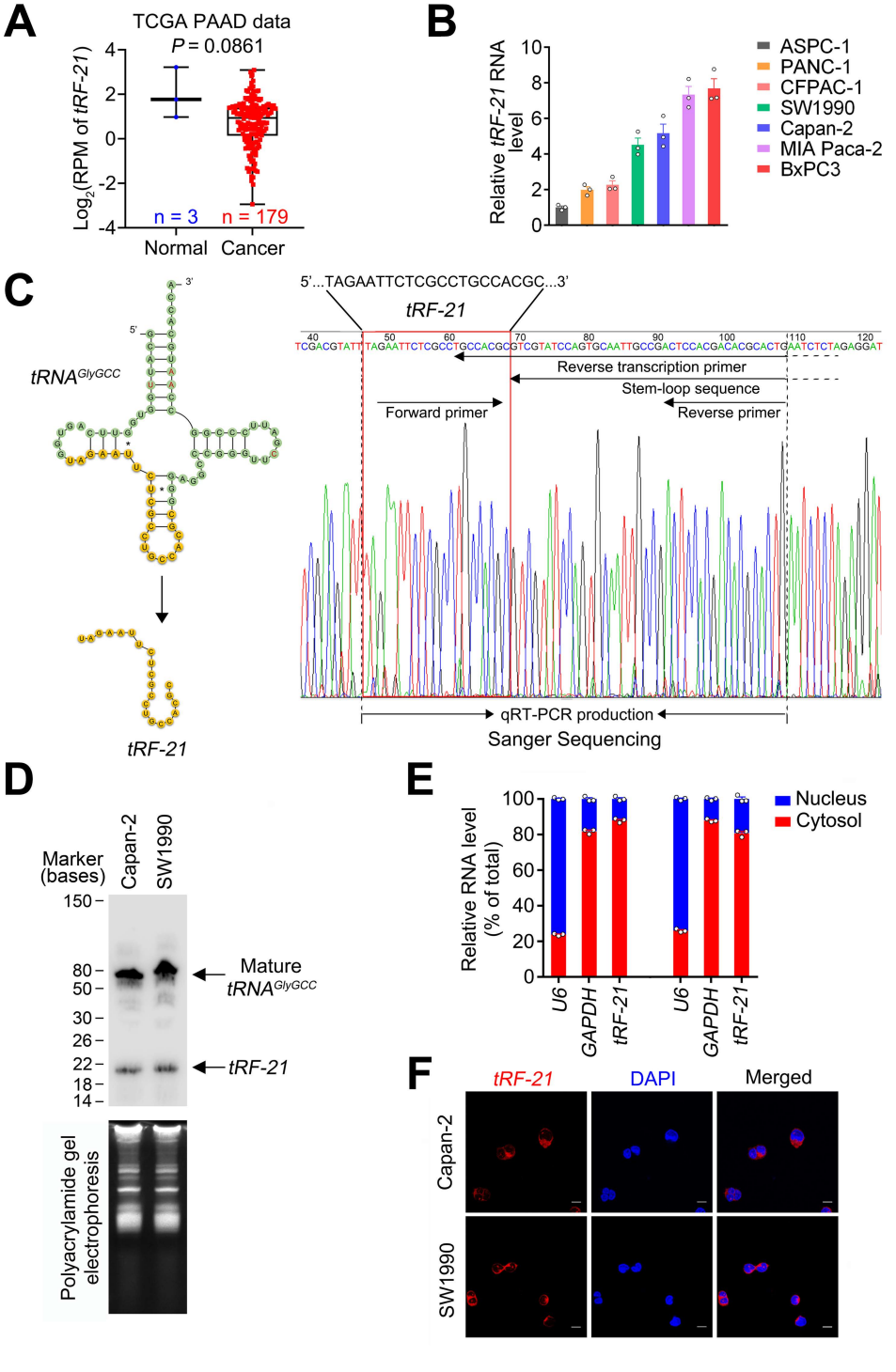

Fig. S1. Identification and characterization of *tRF-21*.

(**A**) *tRF-21* levels in PDAC tumors and adjacent normal tissues. (**B**) Relative *tRF-21* levels in 7 pancreatic cancer cell lines determined by qPCR. (**C**) Diagram and sequence of *tRF-21* derived from mature $tRNA^{GlyGCC}$. Left panel shows diagram of *tRF-21* and right panel shows sanger sequencing of stem-loop production of qRT-PCR. The sequence within the red frame is *tRF-21* and black arrows indicate used primers. (**D**) Northern blot of *tRF-21* in PDAC cells. (**E** and **F**) Analysis of subcellular localization by qPCR (**E**) or RNA FISH (**F**) shows *tRF-21* is mainly located in the cytoplasm of PDAC cells. *U6* and *GAPDH* are respectively nuclear and cytoplasmic markers. Data in (**E**) are mean ± SEM from 3 independent experiments. Scale bars, 10 μm.

Pan et al. Supplementary Figure 2

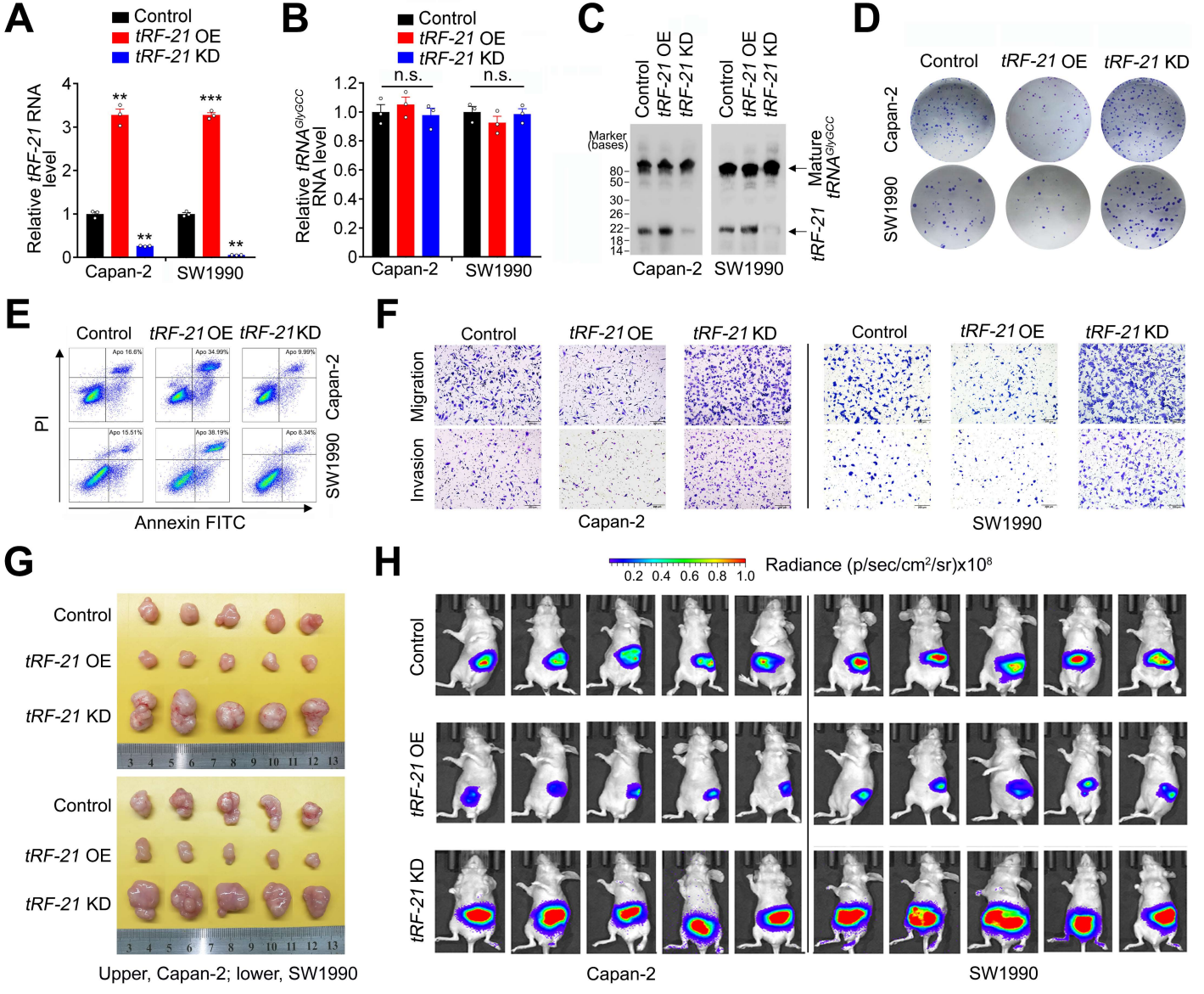

Fig. S2. Effects of *tRF-21* on PDAC cell phenotypes.

(**A**–**C**) Relative *tRF-21* (**A**) and $tRNA^{GlyGCC}$ (**B**) levels by qPCR and northern blot (**C**) in cells with *tRF-21* overexpression (*tRF-21* OE) or silence (*tRF-21* KD). Data are mean ± SEM from 3 independent experiments. **, $P < 0.01$; ***, $P < 0.001$ and n.s., not significant by one-way ANOVA with Dunnett's T3 multiple comparison test. (**D**–**F**) Representative pictures showing the effects of *tRF-21* expression change on colony formation (**D**), apoptosis (**E**) and migration and invasion (**F**) of PDAC cells. Scale bars, 200 μm. (**G**) Effect of *tRF-21* expression change on PDAC xenograft growth in mice. Shown are images of the subcutaneous xenografts at the end of experiments. (**H**) Bioluminescence images showing the effect of *tRF-21* expression change on the tumor burden of mice with orthotopically transplanted PDAC ($n = 5$).

Pan et al. Supplementary Figure 3

A

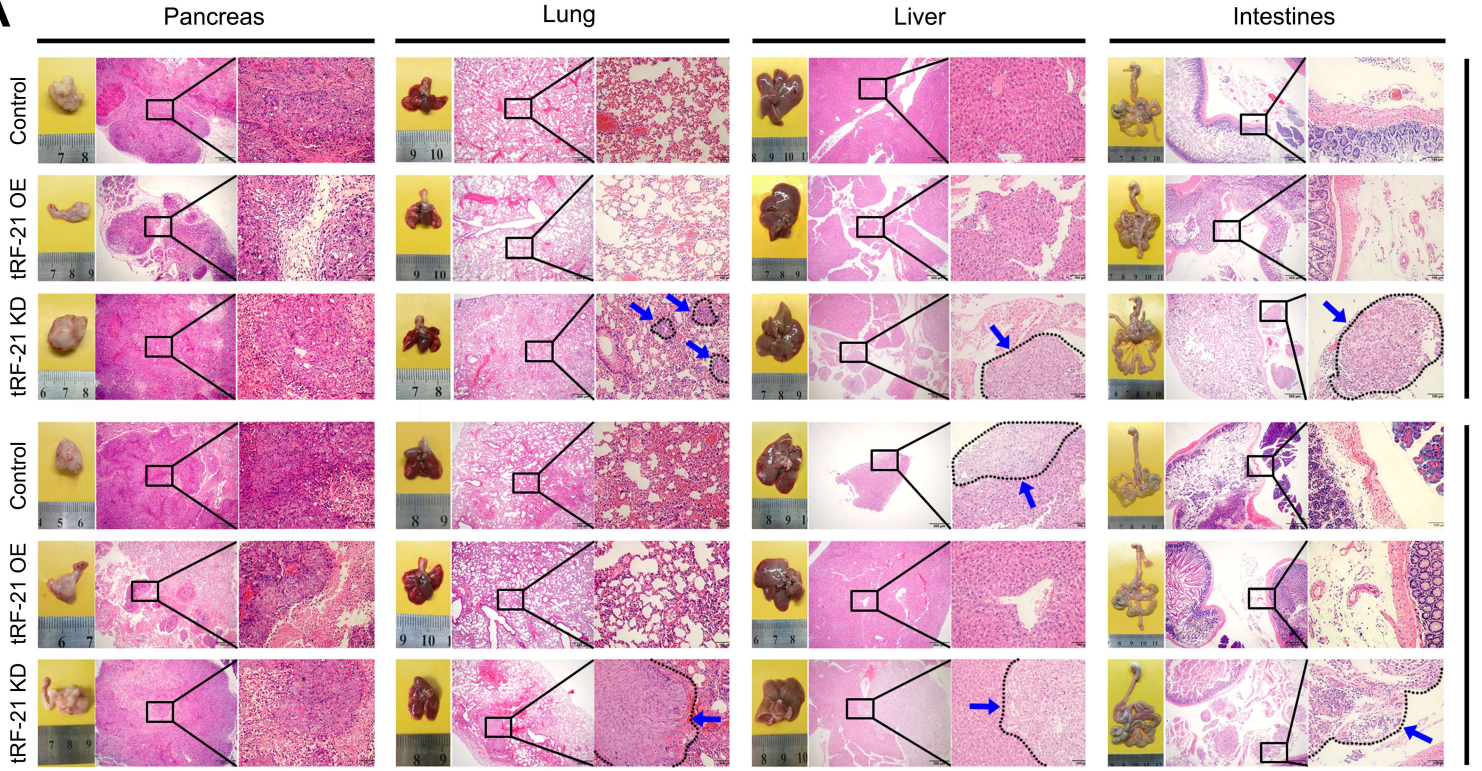

B

Metastasis of xenografts derived from Capan-2 cells

Mouse	Control gruop	*tRF-21* OE group	*tRF-21* KD group
#1	None	None	Lung, liver & mesentery
#2	None	None	Lung & mesentery
#3	None	None	Lung, liver & mesentery
#4	Mesentery	None	Lung, liver & mesentery
#5	None	None	Lung, liver & mesentery
#6	Liver	None	Liver & mesentery
#7	Lung	None	Lung
#8	Mesentery	Mesentery	Lung & mesentery

C

Metastasis of xenografts derived from SW1990 cells

Mouse	Control gruop	*tRF-21* OE group	*tRF-21* KD group
#1	Liver	None	Lung, liver & mesentery
#2	None	None	Lung, liver & mesentery
#3	None	None	Liver & mesentery
#4	Lung & liver	None	Mesentery
#5	None	None	Lung & liver
#6	Lung	None	Liver & mesentery
#7	Liver	None	Lung & mesentery
#8	Lung	Lung	Lung, liver & mesentery

Fig. S3. Effects of *tRF-21* on tumor metastasis in mice with pancreatic transplantation.

(**A**) Histopathological images of tumor metastasis in 4 organs of mice with pancreatic transplantation. The blue arrows in dashed areas indicate tumor lesions. H&E staining; scale bars, 100 and 500 μm, respectively. (**B** and **C**) Organs with metastatic tumors from pancreatic xenograft derived from Capan-2 (**B**) and SW1990 (**C**) cells in each mouse. Quantified data are shown in Fig. 2H.

Pan et al.Supplementary Figure 4

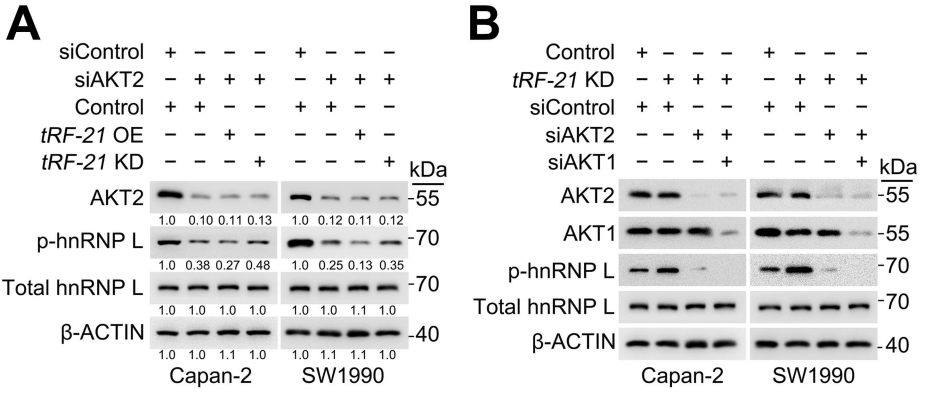

Fig. S4. Activity of AKT1 in hnRNP L phosphorylation.

(**A**) Western blot analysis showing the effects of *tRF-21* expression change on hnRNP L phosphorylation in absence of AKT2. OE, overexpression; KD, knockdown. (**B**) Western blot analysis showing the effects of AKT2 or AKT1 on hnRNP L phosphorylation in absence of *tRF-21*. KD, knockdown.

Pan et al. Supplementary Figure 5

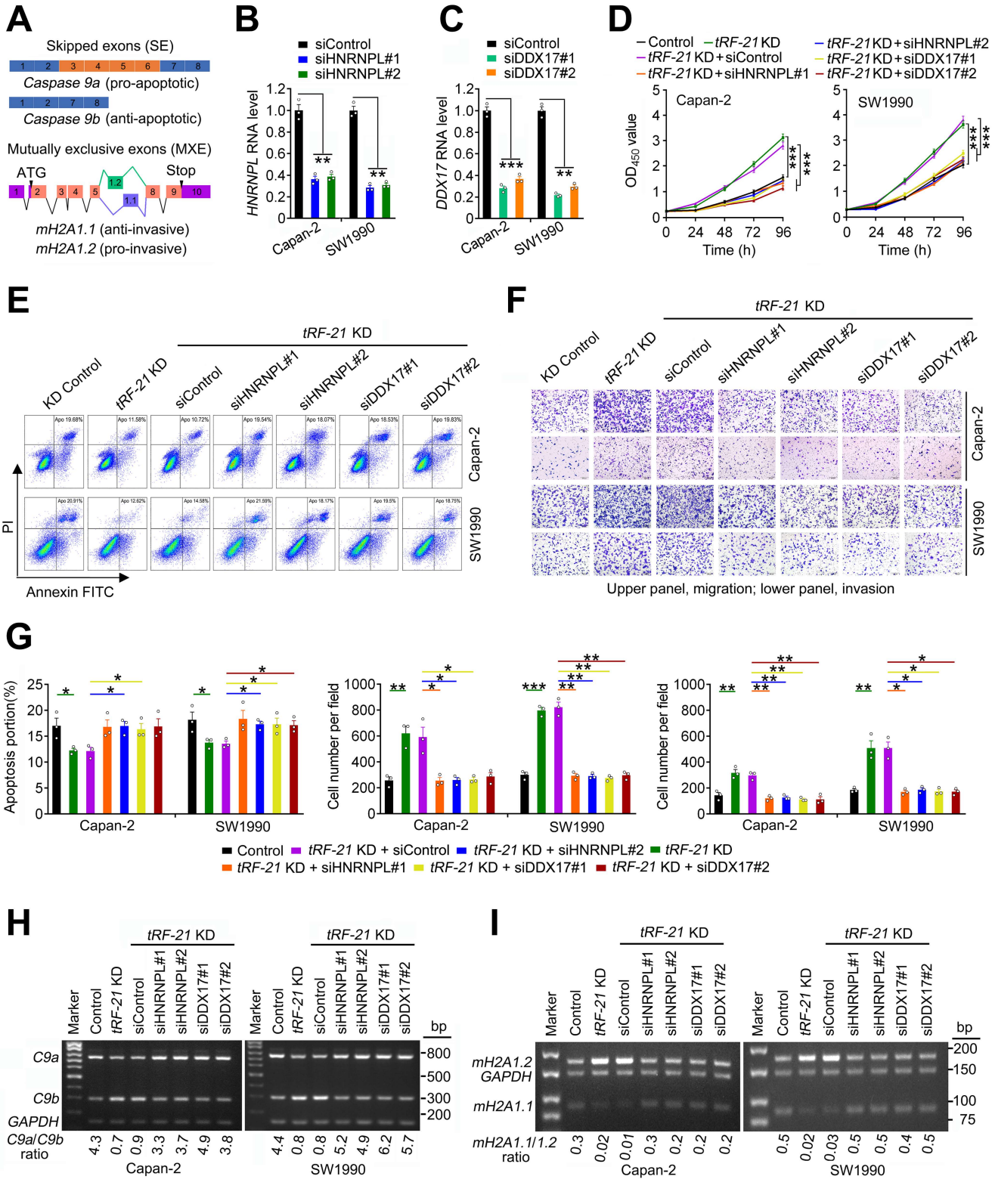

Fig. S5. *tRF-21* suppresses PADC cell proliferation and invasion via *HNRNPL* and *DDX17*.

(**A**) Diagrams of two splice variants of *CASP9* (upper panel) and *mH2A1* mRNA (lower panel) and their opposite functions (22, 23). (**B** and **C**) Relative *HNRNPL* and *DDX17* levels in cells with each of them silenced. (**D**–**G**) Effects of *HNRNPL* or *DDX17* silence on proliferation (**D**), apoptosis (**E**) and migration and invasion (**F**) in cells with *tRF-21* silenced (KD). Scale bars in (**F**), 200 μm; (**G**) shows quantification data of (**E**) and (**F**). (**H** and **I**) Effects of *HNRNPL* or *DDX17* silence on the ratios of *Caspase 9a/9b* (*C9a/C9b*) (**H**) and *mH2A1.1/mH2A1.2* (*mH2A1.1/1.2*) (**I**) mRNAs determined by qRT-PCR in cell with *tRF-21* silenced. Data in (**B**–**D**) and (**G**) are mean ± SEM from at least 3 independent experiments *, $P < 0.05$; **, $P < 0.01$ and ***, $P < 0.001$ by one-way ANOVA with Dunnett's T3 multiple comparison test. *, $P < 0.05$; **, $P < 0.01$ and ***, $P < 0.001$ between Control and *tRF-21* KD group in (**G**) were determined by Student's *t*-test.

Pan et al. Supplementary Figure 6

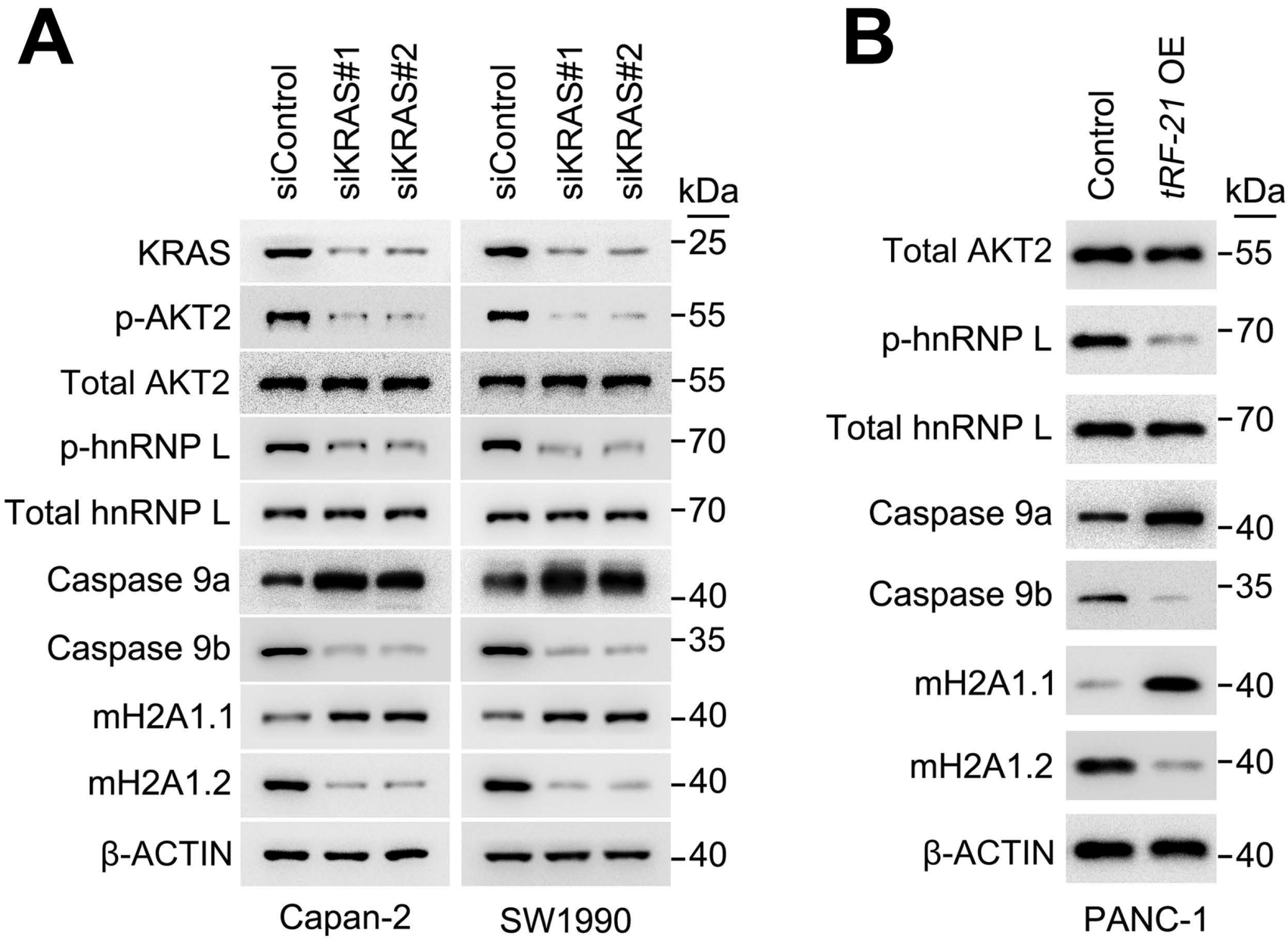

Fig. S6. Effects of *KRAS* and amplified *AKT2* on phosphorylation of hnRNP L and its downstream molecules regulated by *tRF-21*.

(**A**) Western blot analysis showing the effect of *KRAS* knockdown on phosphorylation of AKT2 and the levels of hnRNP L downstream molecules in two PDAC cell lines. (**B**) Western blot analysis showing the effect of *tRF-21* overexpression on phosphorylation of hnRNP L and the levels of its downstream molecules in PANC-1 cells that have *AKT2* amplification.

Pan et al. Supplementary Figure 7

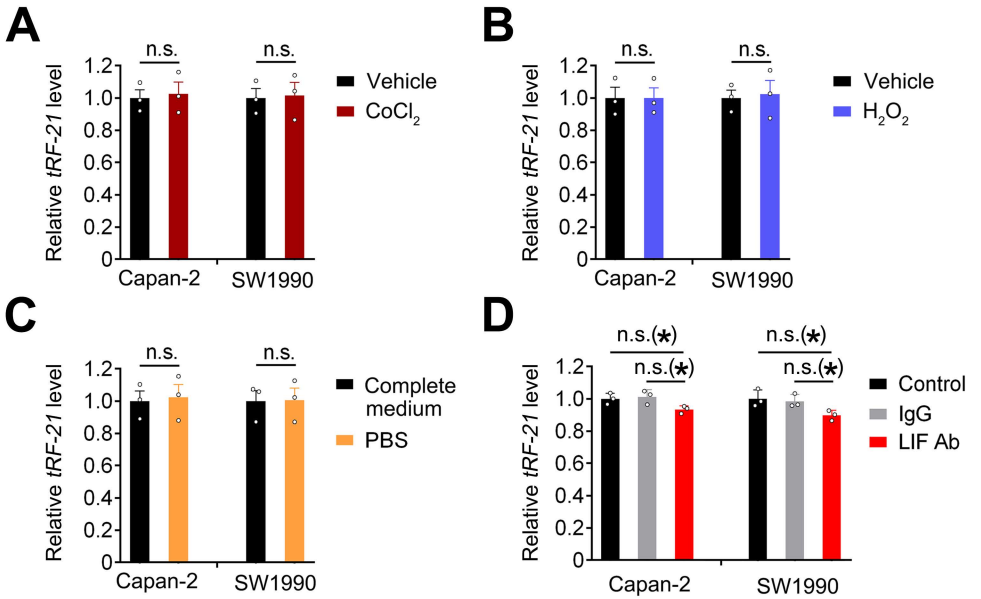

Fig. S7. Effects of different stress conditions on *tRF-21* production in PDAC cells.

(**A-C**) Effects of $CoCl_2$ (50 μM, 24 h; **A**), H_2O_2 (5 mM, 4h; **B**) or PBS (30 min; **C**) on *tRF-21* production. Data in (**A-C**) are mean ± SEM from 3 independent experiments. n.s., not significant by Student's *t*-test compared with corresponding control; (**D**) The *tRF-21* levels in PDAC cells treated with LIF neutralizing antibody (LIF Ab, 2 μg/ml; 1 h). IgG as a negative control. Data are mean ± SEM from 3 independent experiments. n.s., not significant were determined by one-way ANOVA with Dunnett's T3 multiple comparison test; (*), $P < 0.05$ by Student's *t*-test compared with corresponding control.

Pan et al. Supplementary Figure 8

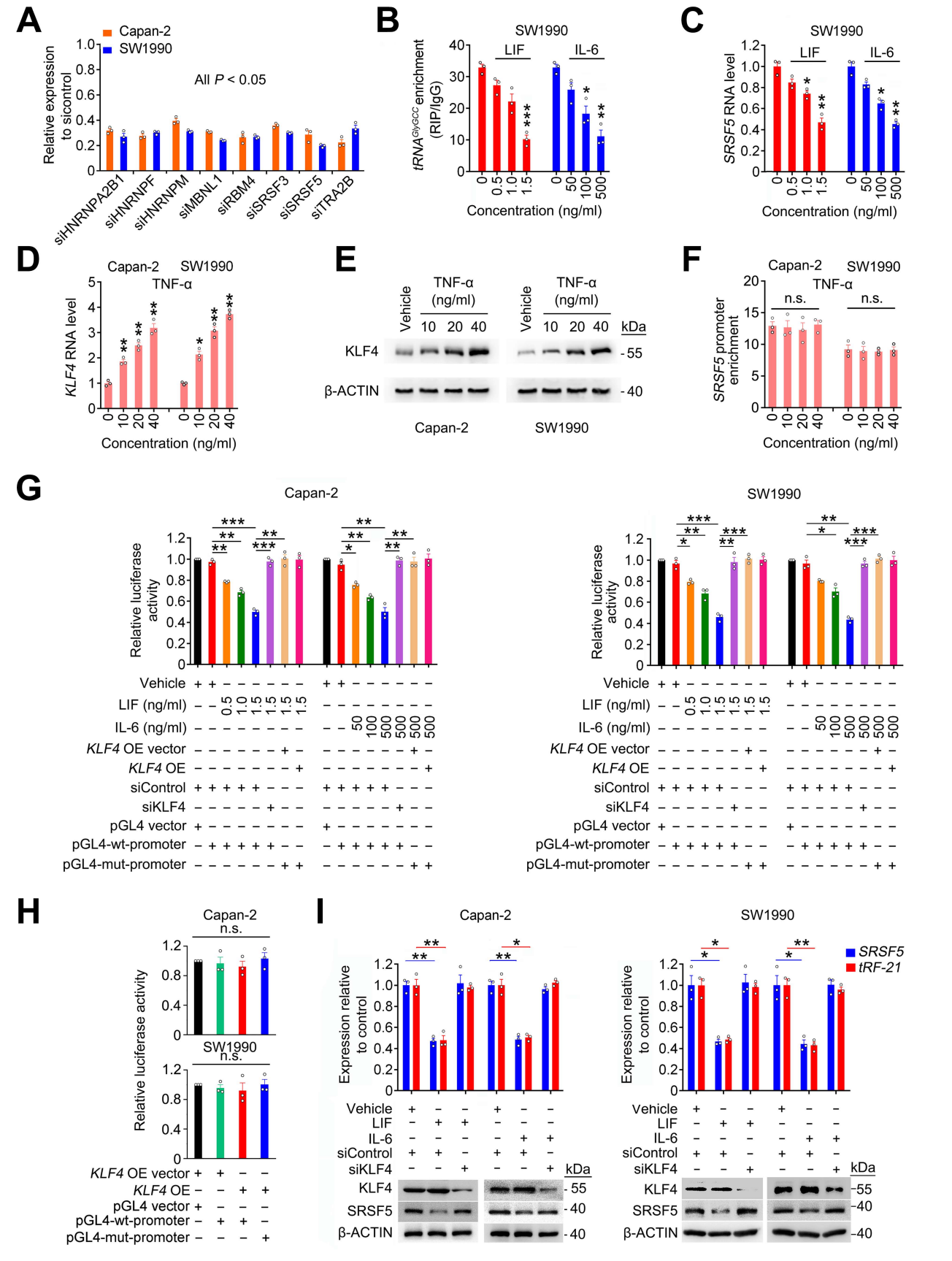

Fig. S8. LIF and IL-6 enhances KLF4 binding to *SRSF5* promoter.

(**A**) Silencing efficiency of 8 RNA binding proteins in PDAC cells by small interfering RNA. Data are mean ± SEM from 3 independent experiments. (**B**) Association of SRSF5 with $tRNA^{GlyGCC}$ determined by RNA immunoprecipitation (RIP) assays in SW1990 cells cultured with LIF or IL-6. (**C**) *SRSF5* levels in SW1990 cells treated with LIF or IL-6. (**D** and **E**) Effects of TNF-α treatment on *KLF4* mRNA (**D**) and protein (**E**) expression levels in Capan-2 and SW1990 cells. (**F**) ChIP assays showing binding of KLF4 to the *SRSF5* promoter in cells treated with TNF-α at various concentrations. (**G**) Luciferase reporter gene expression in PDAC cells co-transfected with indicated plasmids or siRNAs in the presence or absence of LIF or IL-6. OE, overexpression; pGL4-wt-promoter, pGL4-SRSF5-wt-promoter; pGL4-mut-promoter, pGL4-SRSF5-mut-promoter. (**H**) Luciferase reporter gene expression in PDAC cells co-transfected with indicated plasmids in the absence of LIF or IL-6. OE, overexpression; pGL4-wt-promoter, pGL4-SRSF5-wt-promoter; pGL4-mut-promoter, pGL4-SRSF5-mut-promoter. (**I**) Relative *tRF-21* and *SRSF5* levels in PDAC cells with or without *KLF4* silencing in the presence of LIF or IL-6 (upper panel). *KLF4*-silence efficiency and SRSF5 protein level are shown in lower panels. Data in (**A**–**D**) and (**F**–**I**) are mean ± SEM from at least 3 independent experiments. *, $P < 0.05$; **, $P < 0.01$, ***, $P < 0.001$ and n.s., not significant by one-way ANOVA with Dunnett's T3 multiple comparison test.

Pan et al. Supplementary Figure 9

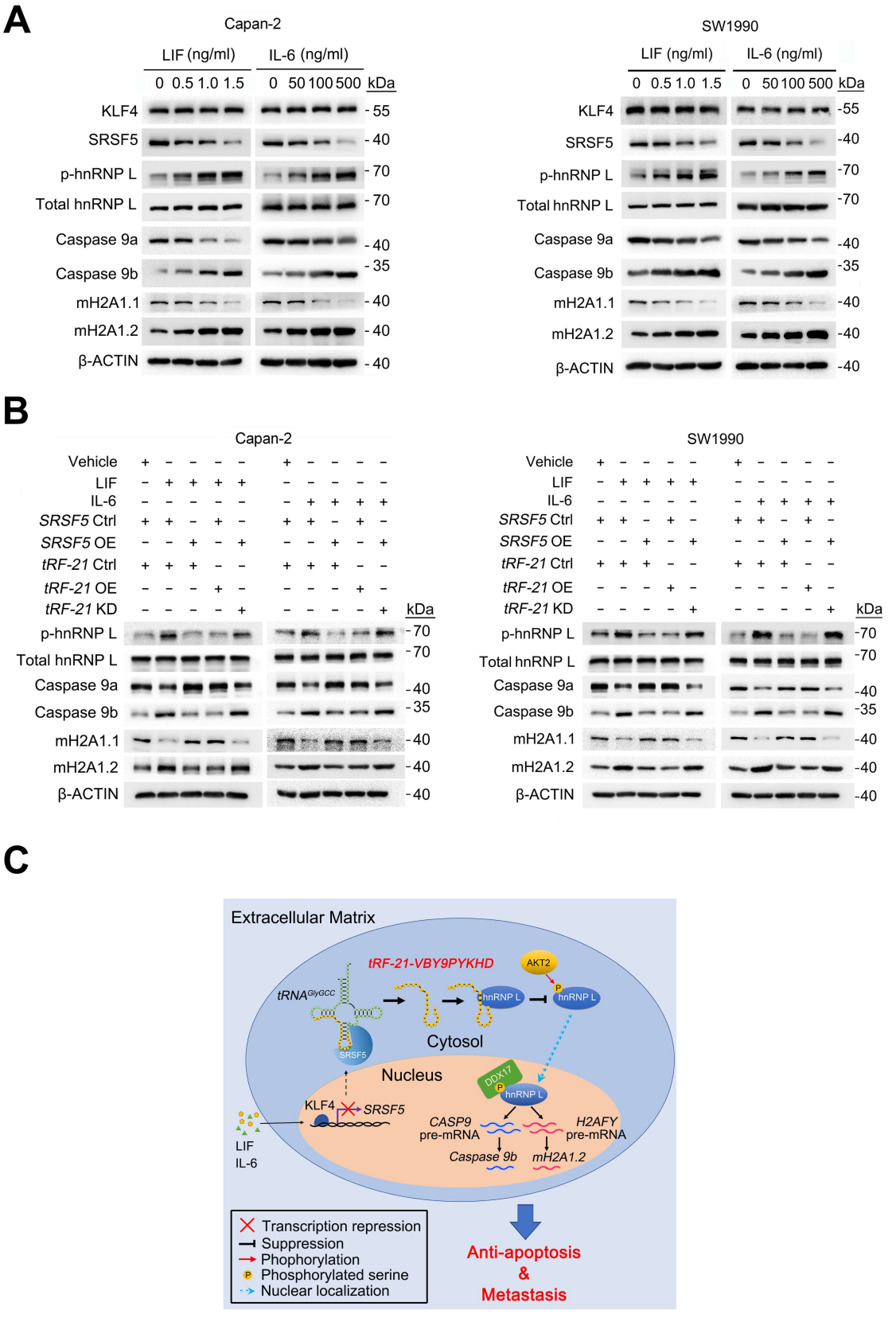

Fig. S9. Validation of LIF/IL-6-KLF4-SRSF5-hnRNP L-Caspase 9/mH2A1 regulatory axis in PDAC cells.

(**A**) Western blot analysis of KLF4, SRSF5, hnRNP L, p-hnRNP L, Caspase 9a, Caspase 9b, mH2A1.1 and mH2A1.2 in PDAC cells cultured with LIF or IL-6 at different concentrations. (**B**) Western blot analysis showing the effects of *SRSF5* or *tRF-21* on hnRNP L-Caspase 9/mH2A1 regulatory axis in PDAC cells cultured with LIF (1.5 ng/ml) or IL-6 (500 ng/ml). Ctrl, control; KD, knockdown. (**C**) A proposed mechanistic model showing the inhibitory effect of inflammatory cytokine LIF or IL-6 on *tRF-21* production and consequential PDAC progression. Attenuation of *tRF-21* enhances hnRNP L activation by AKT2, which preferentially splices *CASP9* and *mH2A1* to form anti-apoptotic *Caspase 9b* and metastatic *mH2A1.2*.

Pan et al. Supplementary Figure 10

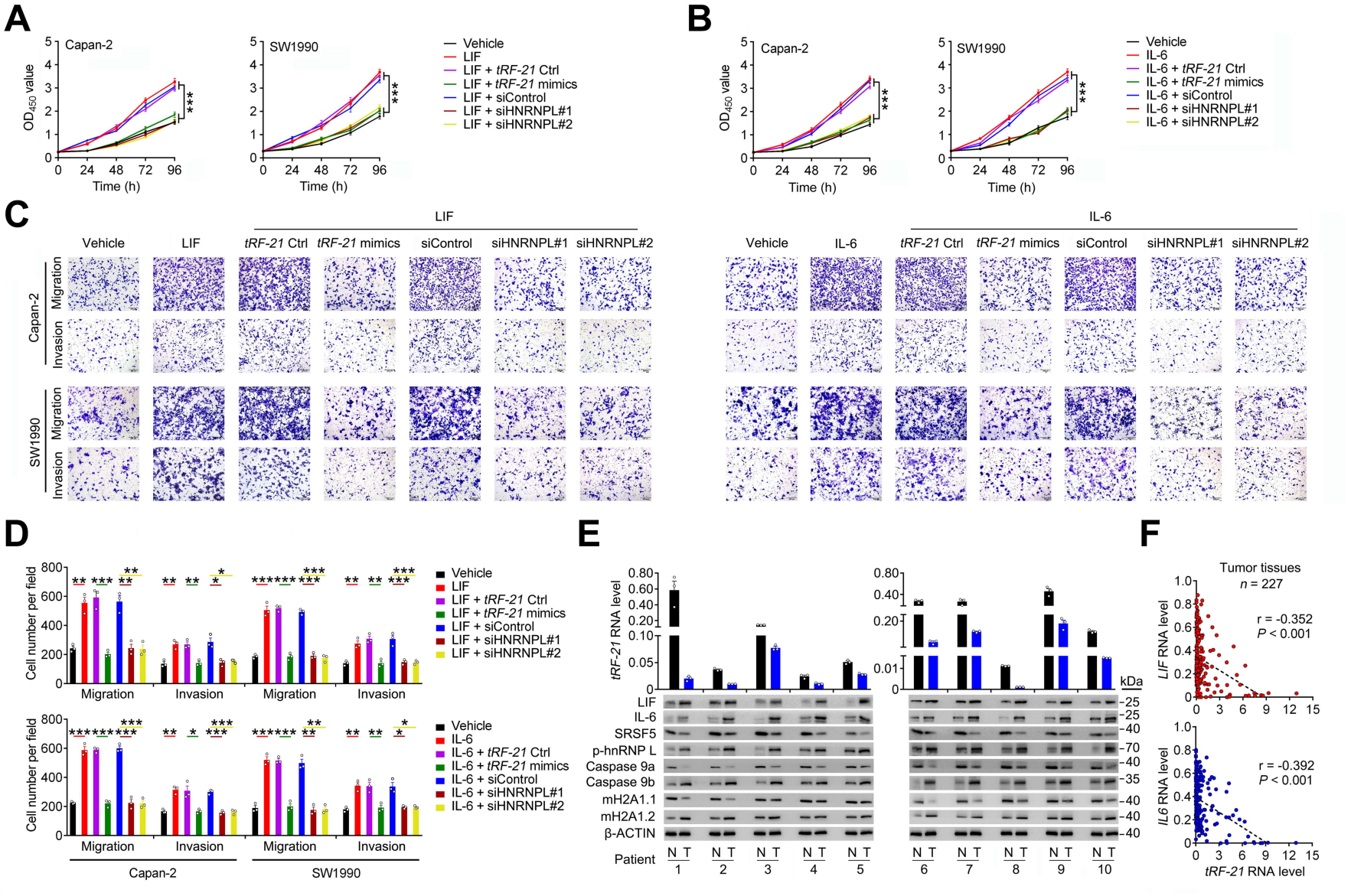

Fig. S10. LIF and IL-6 promotes PDAC cell malignant phenotypes via *tRF-21* and *HNRNPL*.
(**A** and **B**) Effects of *tRF-21* mimics or *HNRNPL* silence on cell proliferation in the presence of LIF (**A**) or IL-6 (**B**). (**C** and **D**) Effects of *tRF-21* mimics or *HNRNPL* silence on cell migration and invasion. Shown are representative images of transwell assays (**C**) and statistics of the quantification data (**D**). Scale bar, 200 μm. The concentration of LIF and IL-6 used was 1.5 ng/ml and 500 ng/ml, respectively. Ctrl, control. (**E**) qRT-PCR (upper panels) and western blot (lower panels) analysis of *tRF-21* and proteins in the regulatory axis in 10 pairs of matched clinical pancreatic cancer and normal tissue samples. N, normal; T, tumor. (**F**) Correlations between *tRF-21* and *LIF* or *IL6* RNA levels in 227 pancreatic tumor tissues by Pearson's test. Data in (**A**), (**B**) and (**D**) are mean ± SEM from at least 3 independent experiments *, $P < 0.05$; **, $P < 0.01$ and ***, $P < 0.001$ by one-way ANOVA with Dunnett's T3 multiple comparison test.

Pan et al. Supplementary Figure 11

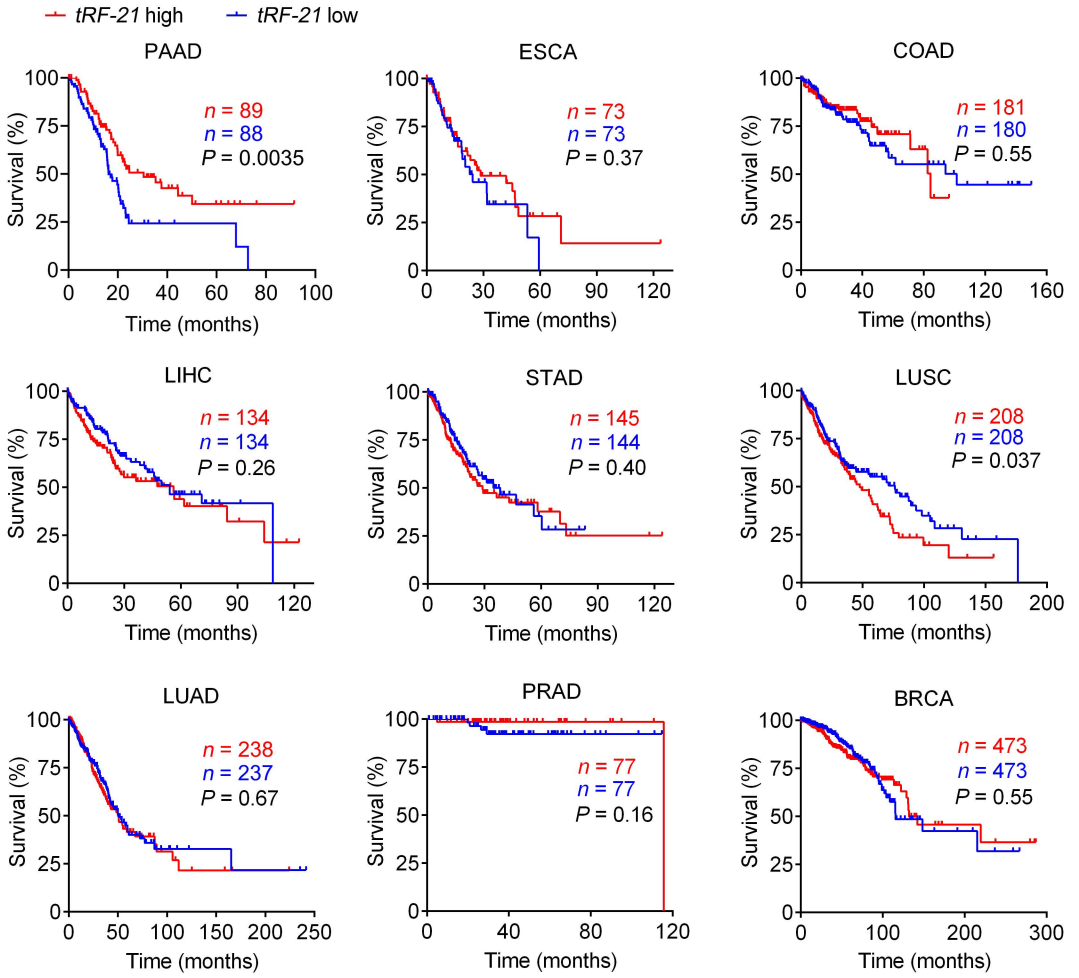

Fig. S11. Correlations between *tRF-21* levels in tumors and survival time in patients with different cancer types in TCGA database.

Shown are Kaplan-Meier survival curves with log-rank *P* values for 9 cancer types. Significant correlation is seen only in PAAD and LUSC; however, in LUSC patients, low level of *tRF-21* was associated with better survival in patients. PAAD, pancreatic cancer; ESCA, esophageal carcinoma; COAD, colon adenocarcinoma; LIHC, liver hepatocellular carcinoma; STAD, stomach adenocarcinoma; LUSC, lung squamous cell carcinoma; LUAD, lung adenocarcinoma; PRAD, prostate adenocarcinoma; BRCA, breast invasive carcinoma.

Pan et al. Supplementary Figure 12

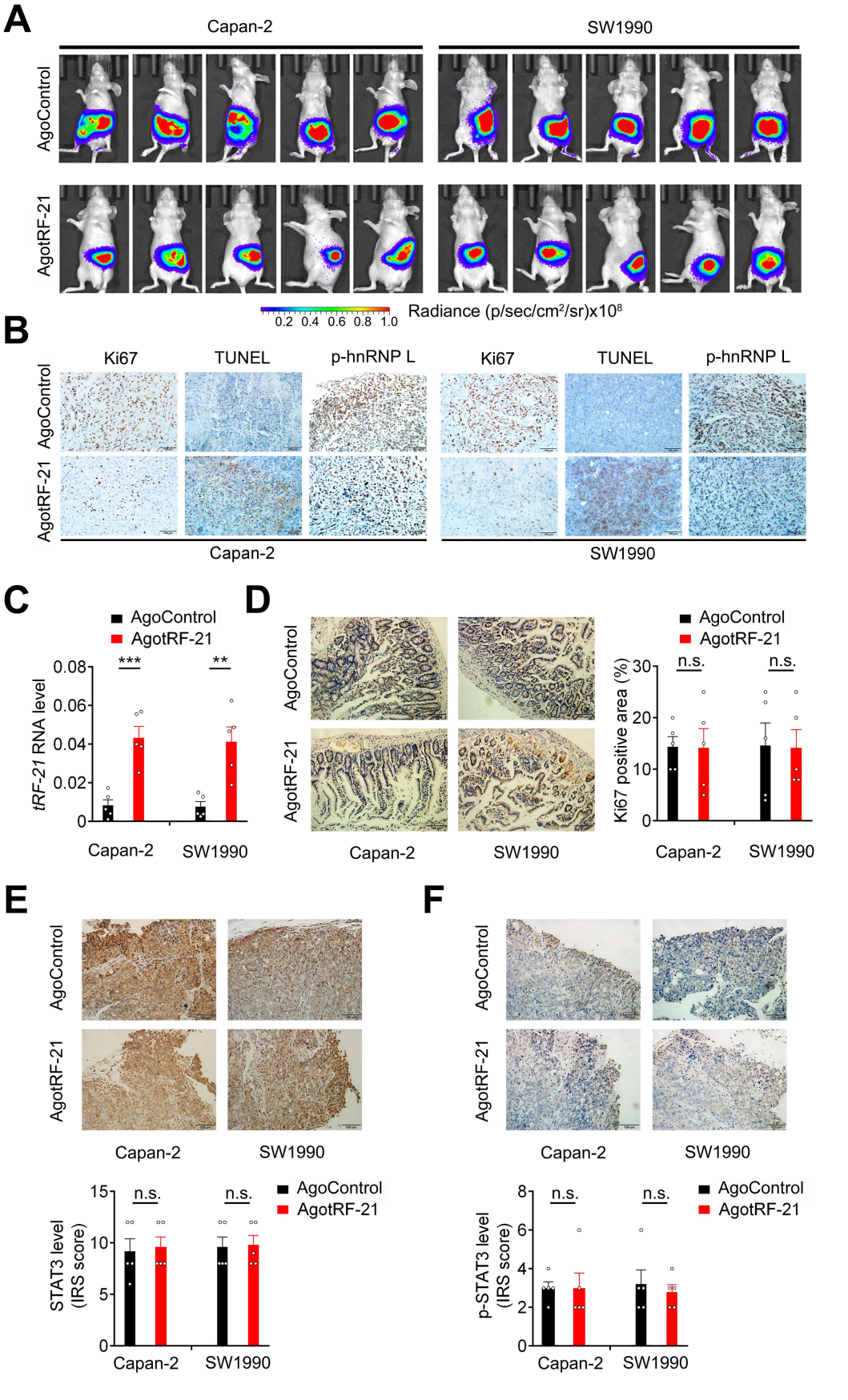

Fig. S12. Therapeutic effect of *tRF-21* on pancreatic xenografts in mice.

(**A**) Bioluminescence imaging of mice with different treatment (*n* = 5 for each group). Refer to Figure 9B. (**B**) Immunohistochemical (IHC) analysis of Ki67, TUNEL and p-Ser52-hnRNP L (p-hnRNP L) in orthotopically implanted PDACs with different treatment. Shown are representative IHC images of IHC staining. Scale bar, 100 μm. (**C**) Relative *tRF-21* levels in pancreatic xenografts of mice with different treatment. Data are mean ± SEM from 5 mice in each group. **, $P < 0.01$ and ***, $P < 0.001$ of Student's *t*-test compared with agoControl. (**D**) Immunohistochemical staining of Ki67 in intestines of mice with pancreatic xenograft. Shown are representative images (left panel) and statistics (right panel). n.s., not significant of Student's *t*-test compared with agoControl. Scale bar, 100 μm. (**E** and **F**) Immunohistochemical staining of STAT3 (**E**), p-Tyr705-STAT3 (p-STAT3) (**F**) in pancreatic xenografts. Shown are representative images (upper panels) and statistics (lower panels). Scale bars, 100 μm. Data in (**C-F**) are mean ± SEM from 5 mice in each group. The differences in (**E** and **F**) were determined by Wilcoxon test.

Pan et al. Supplementary Figure 13

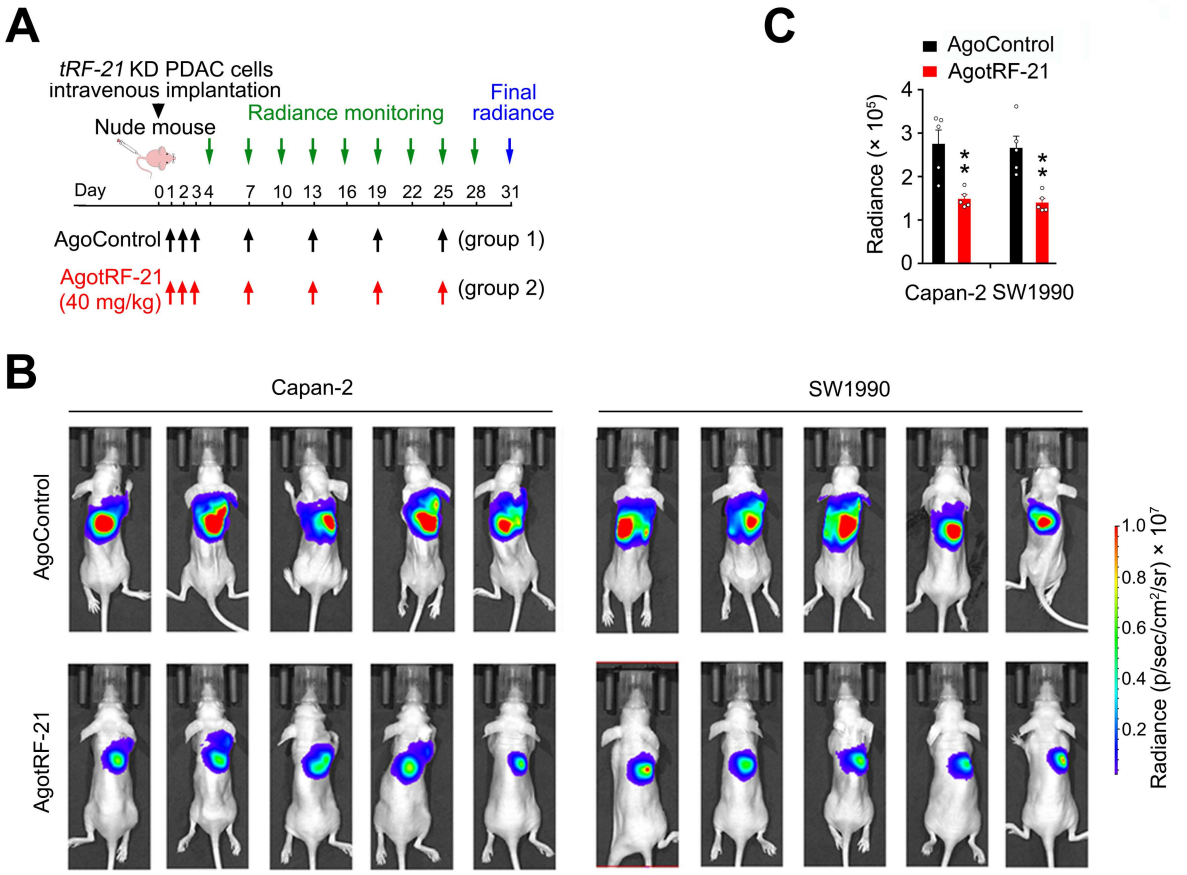

Fig. S13. Therapeutic effect of *tRF-21* on lung colonization in mice.

(**A**) Schematic for treatment of colonization in the lungs of PDAC cells with *tRF-21*-knockdown with agotRF-21 or agoControl. The chemicals were given intravenously. Colored arrows indicate dosing and tumor radiance monitoring time points. (**B** and **C**) Analysis of tumor cell colonization extent in mice with different treatment. Shown are bioluminescence imaging (**B**) and quantitative fluorescent intensities (**C**). Data in (**C**) are mean ± SEM from 5 mice in each group. **, $P < 0.01$ of Student's *t*-test compared with agoControl.

Pan et al. Supplementary Figure 14

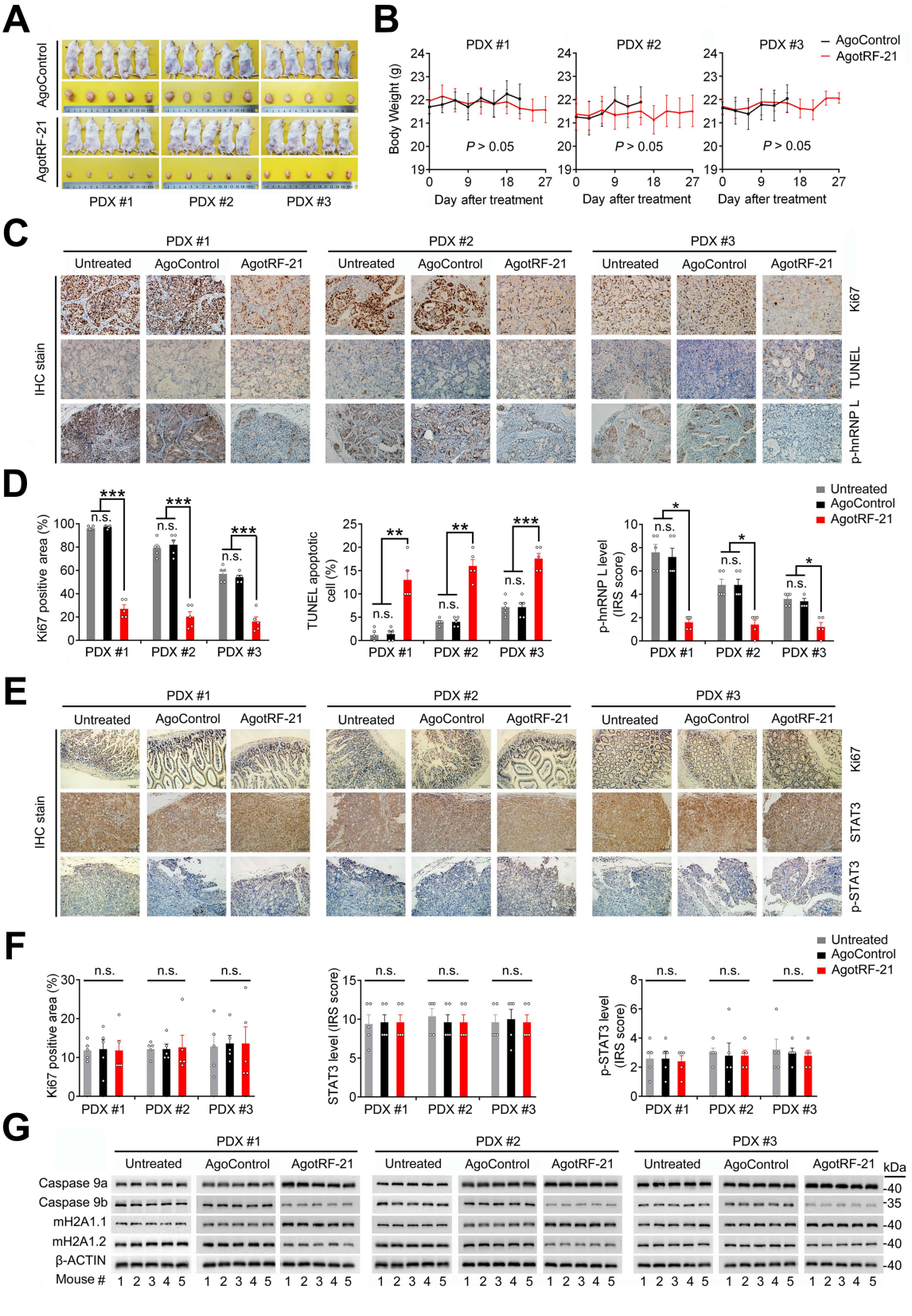

Fig. S14. Therapeutic effect of *tRF-21* on patient-derived xenografts (PDXs) in mice.

(**A**) Pictures of mice with PDX treated with agotRF-21 or agoControl. (**B**) Bodyweight gain of mice carrying PDX treated with agotRF-21 or agoControl. (**C** and **D**) Immunohistochemical staining of Ki67, TUNEL and p-Ser52-hnRNP L (p-hnRNP L) in PDXs. Shown are representative images (**C**) and statistics (**D**). Scale bar, 100 μm. (**E** and **F**) Immunohistochemical staining of Ki67 in mouse intestines and STAT3, p-Tyr705-STAT3 (p-STAT3) in PDXs. Shown are representative images (**E**) and statistics (**F**). Scale bar, 100 μm. (**G**) Western blot analysis of Caspase 9a, Caspase 9b, mH2A1.1 and mH2A1.2 in PDXs of mice. Data in (**D**) and (**F**) are mean ± SEM from 5 mice in each group. ***, $P < 0.001$ of one-way ANOVA with Dunnett's T3 multiple comparison test in (**D,** left and middle panels) and (**F,** left panel). n.s., not significant. *, $P < 0.05$ and **, $P < 0.01$ by one-way ANOVA with Dunn's multiple comparison test in (**D,** right panel) and (**F,** middle and right panels).

Pan et al. Supplementary Figure 15

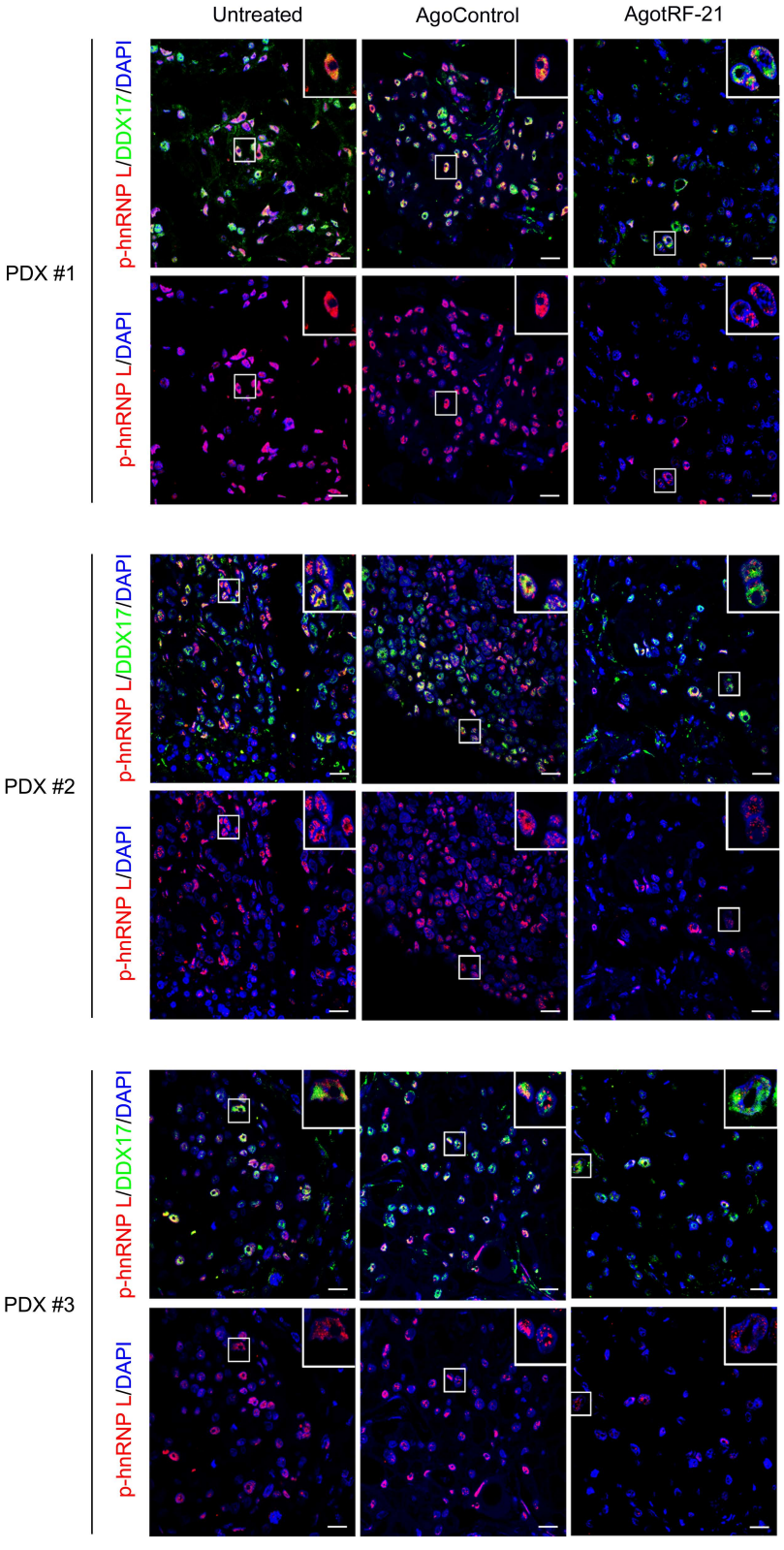

Fig. S15. Representative immunofluorescence images of p-hnRNP L and p-hnRNP L/DDX17 co-staining in PDXs. Scale bars, 20 μm. Refer to Figure 9H.

Pan et al. Supplementary Figure 16

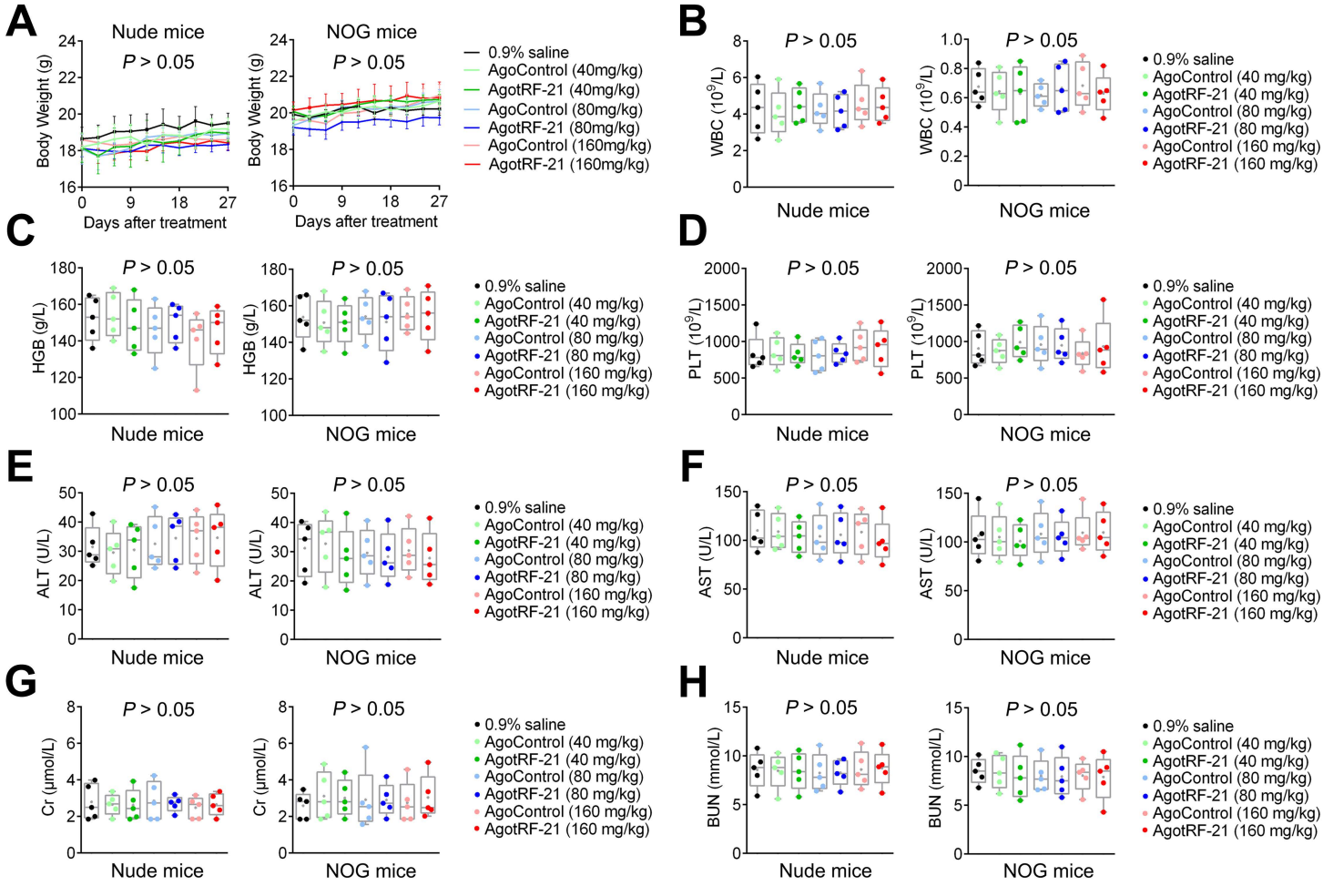

Fig. S16. Evaluation of agotRF-21 toxicity in mice.

(**A**) Bodyweight gains of nude mice (left panel) and NOG mice (right panel) with different treatment as indicated in the figure legend key. (**B**–**D**) AgotRF-21 treatment had no effect on blood count. Blood sample of each nude mouse (left panel) and NOG mice (right panel) was collected from the retro-orbital plexus on the last day of the experiments and the white blood cell (WBC)(**B**), hemoglobin (HGB) (**C**) and platelet (PLT) (**D**) were analyzed. (**E**–**H**) AgotRF-21 treatment for 4 weeks had no toxicity to the liver (**E**–**F**) and kidney (**G**–**H**) of nude mice (left panel) and NOG mice (right panel) as indicated by serum levels of alanine transaminase (ALT), aspartate aminotransferase (AST), creatinine (Cr) and blood urea nitrogen (BUN). Data are mean ± SEM from 5 mice of each species and analyzed by one-way ANOVA with Dunnett's T3 multiple comparison test.

Fig. S17. Uncropped blots and gels in this study.

Full unedited gel for Figure 3

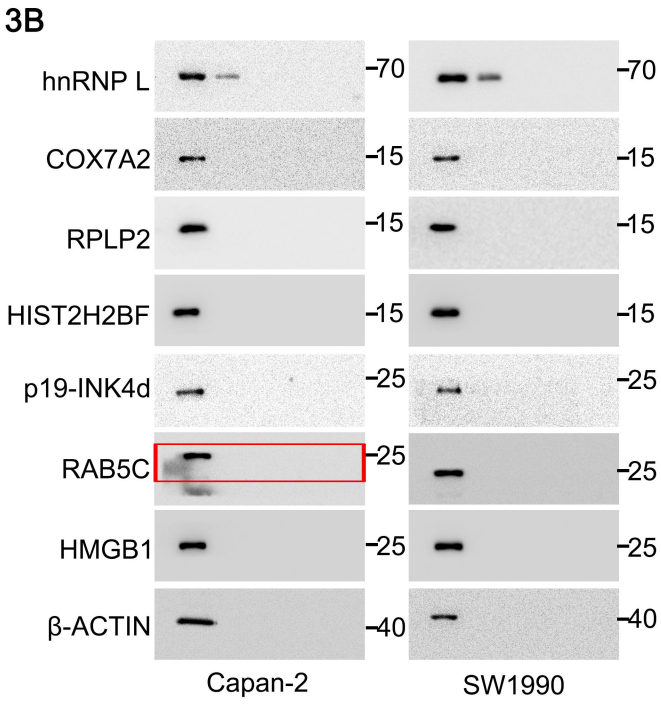

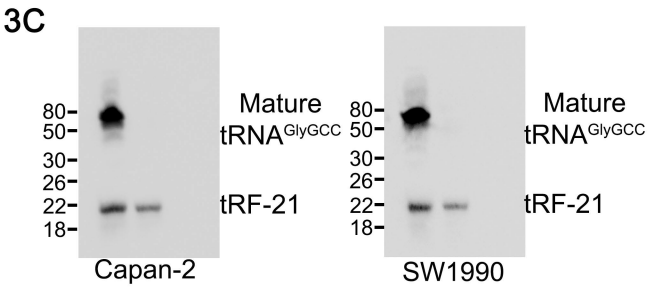

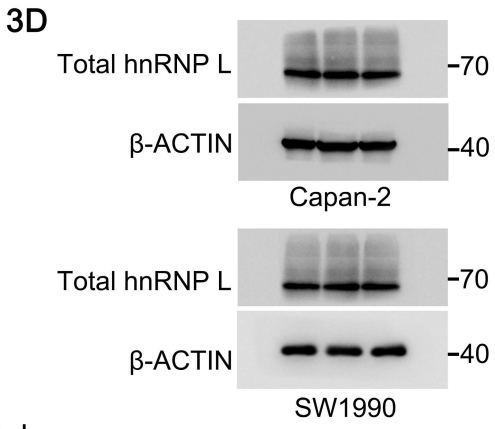

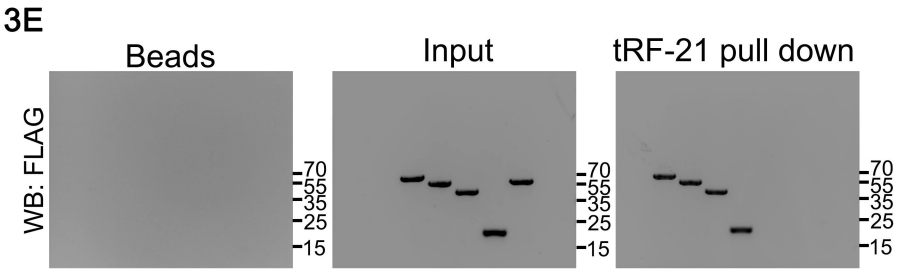

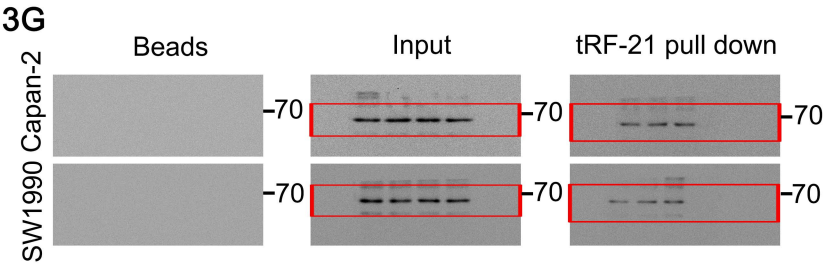

Full unedited gel for Figure 4

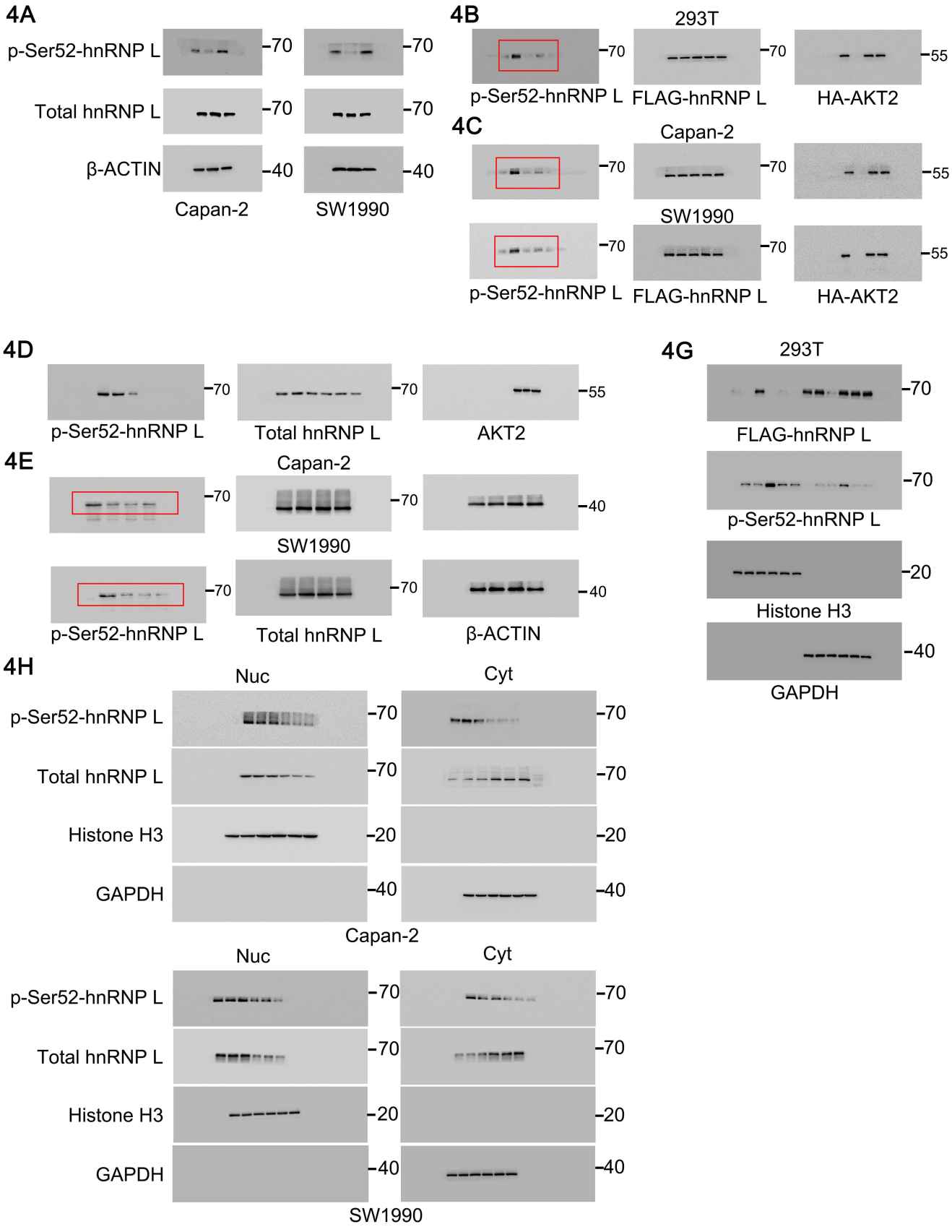

Full unedited gel for Figure 5

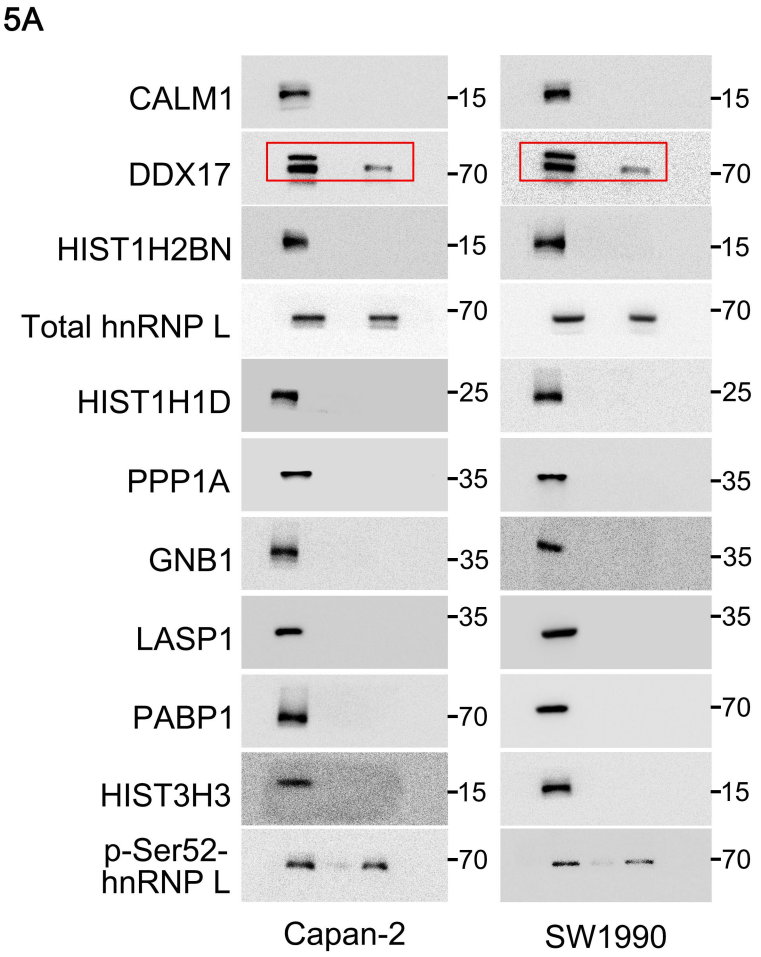

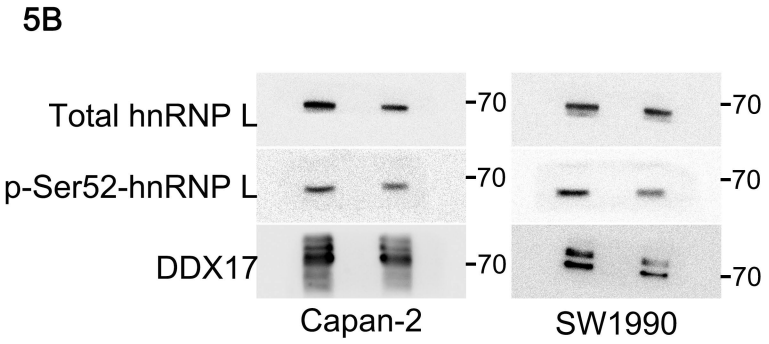

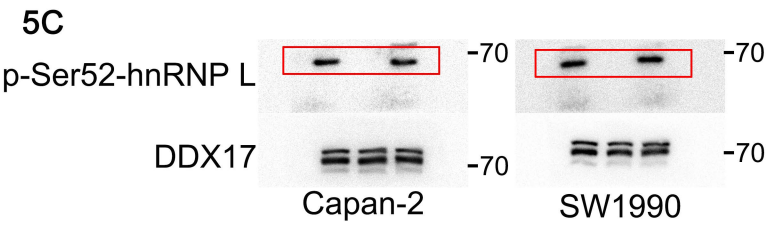

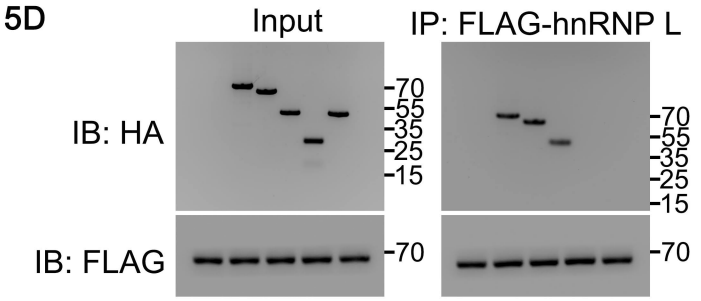

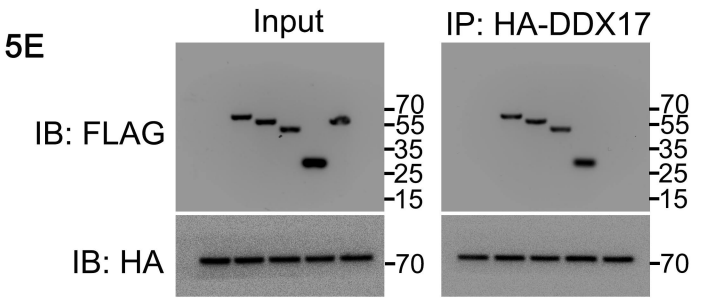

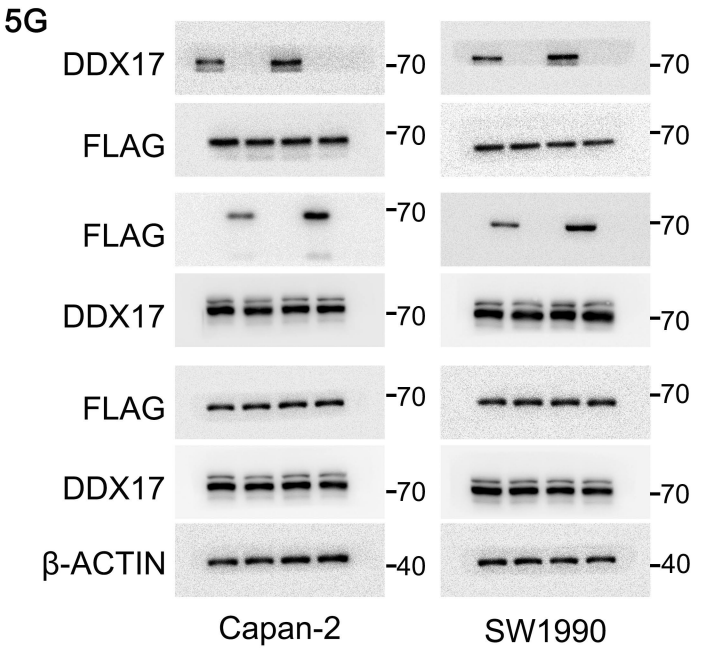

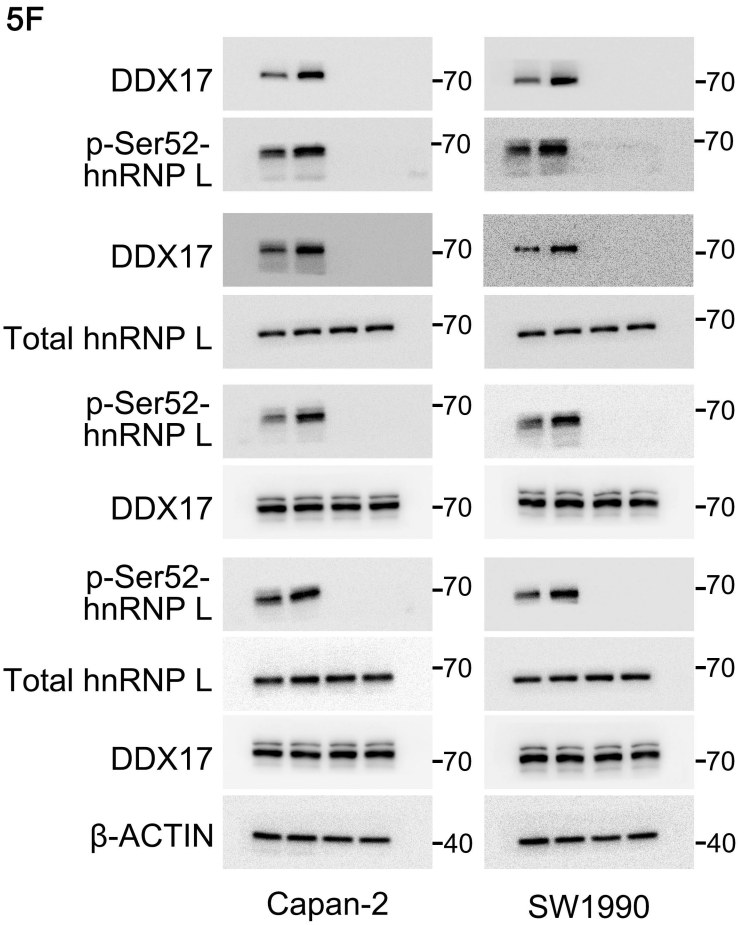

Full unedited gel for Figure 6

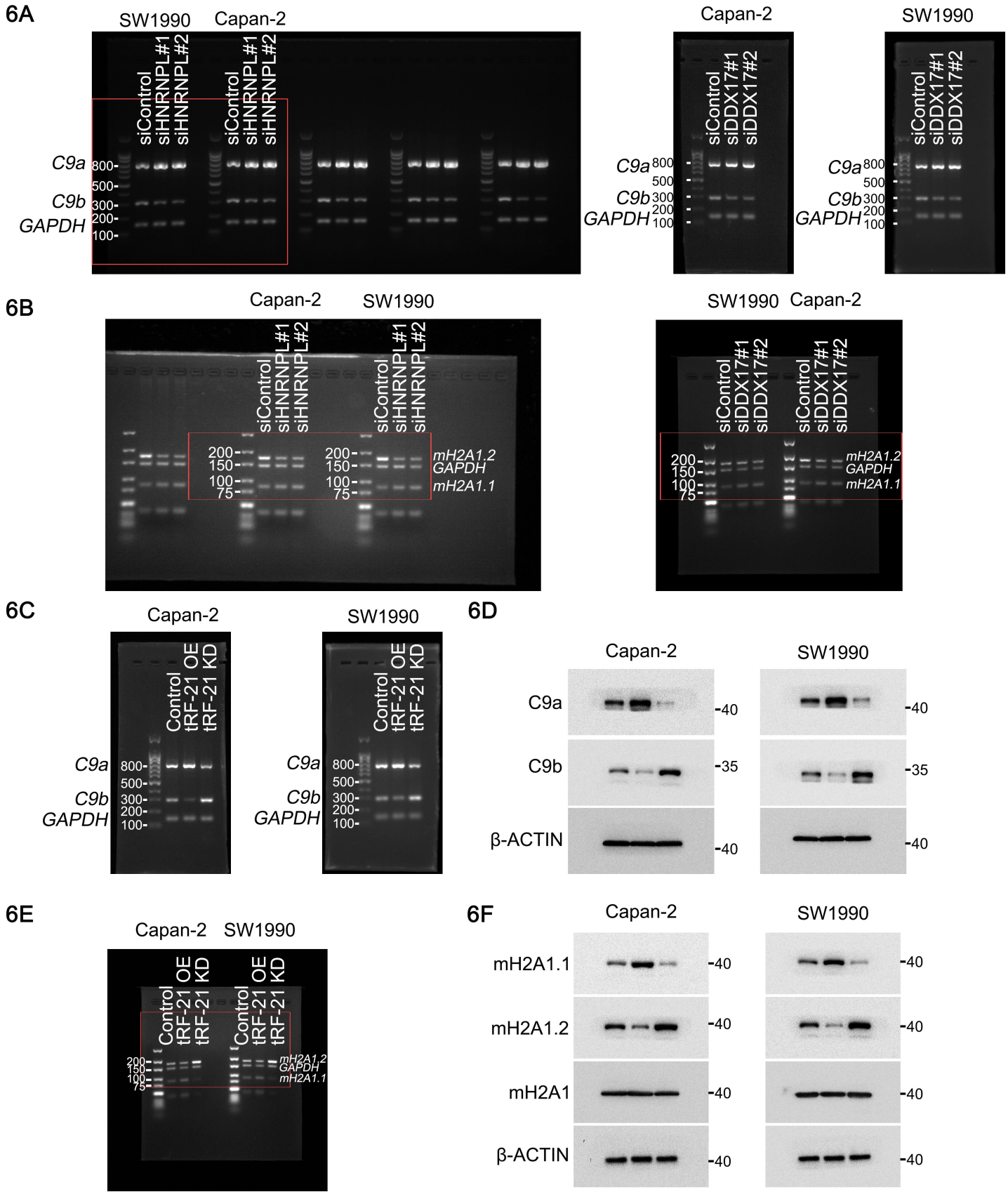

Full unedited gel for Figures 7 and 8

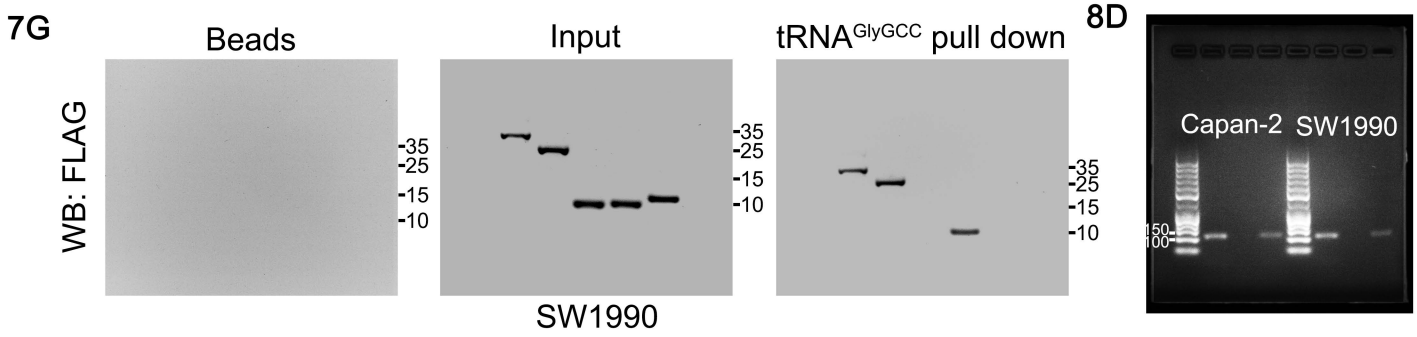

Full unedited gel for Supplementary Figures 1-5

S1D

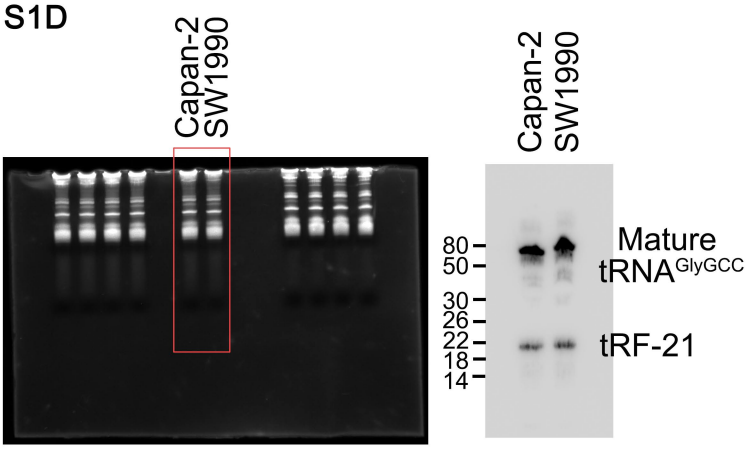

S2C

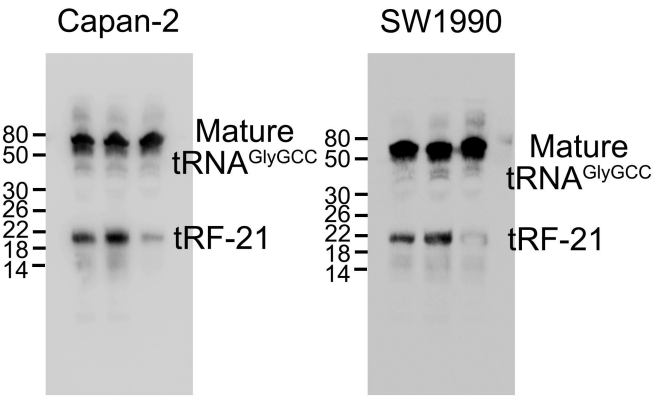

S4A

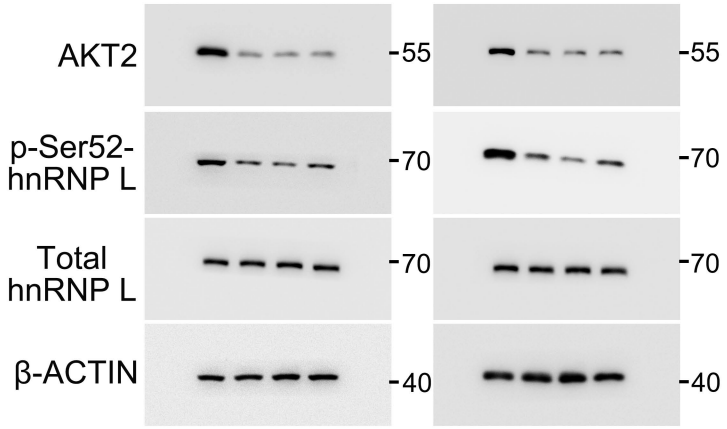

S4B

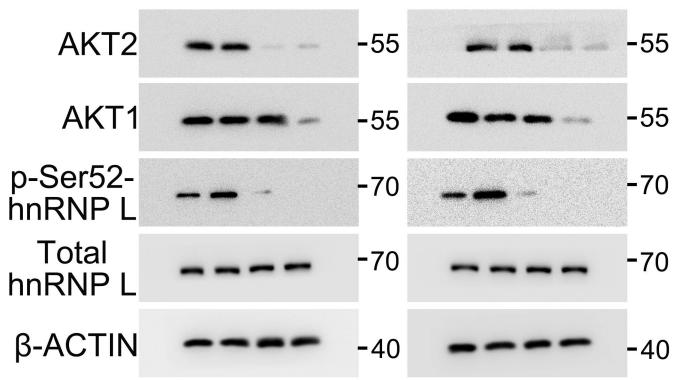

S5H

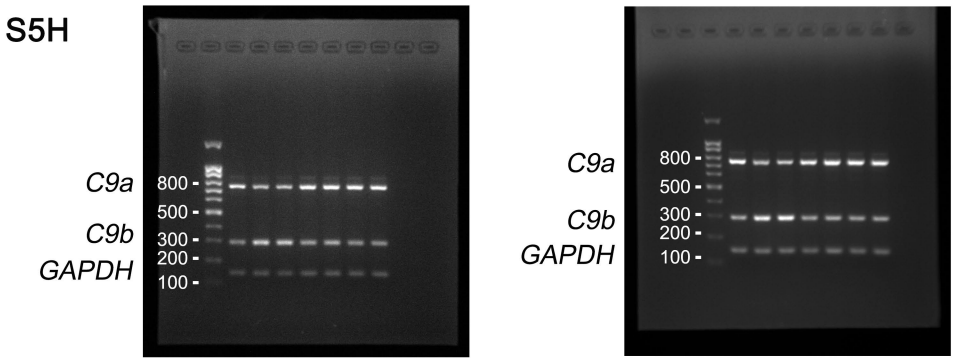

S5I

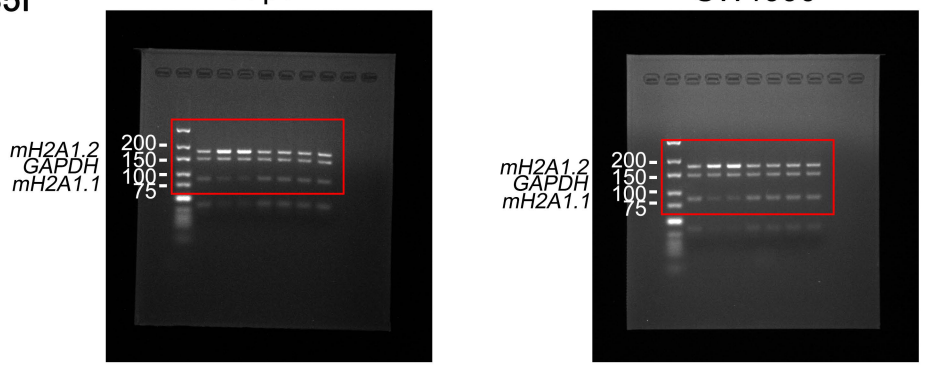

Full unedited gel for Supplementary Figures 6 and 8

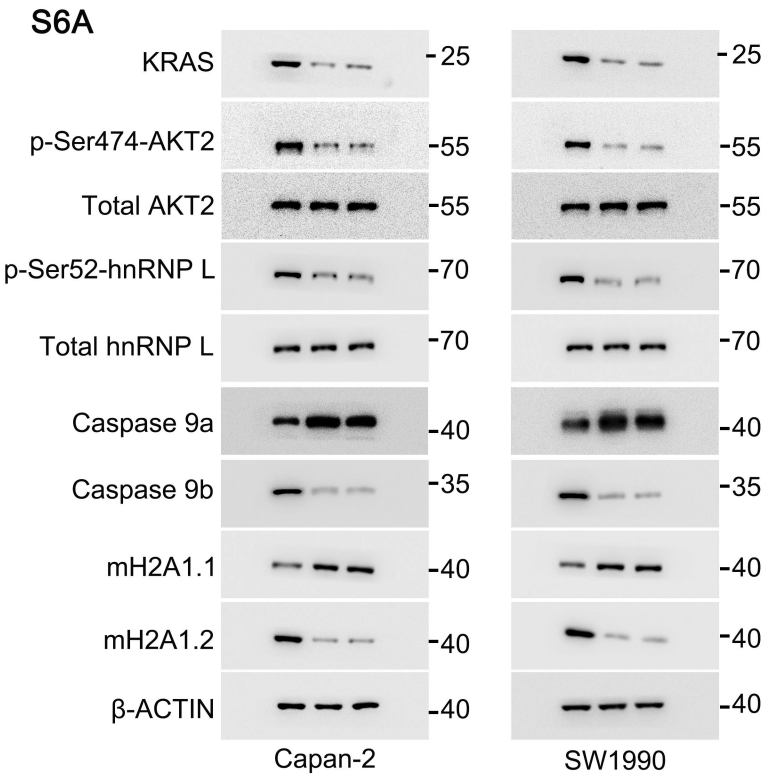

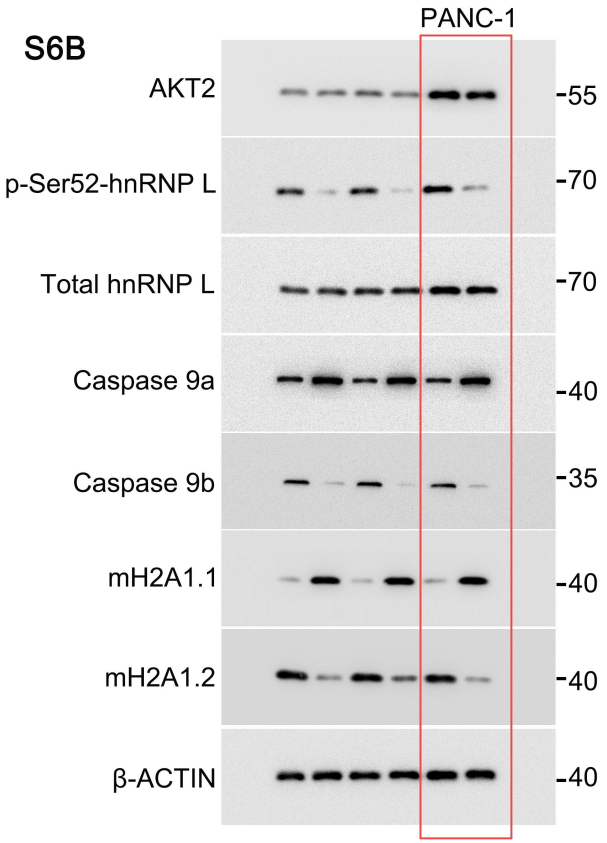

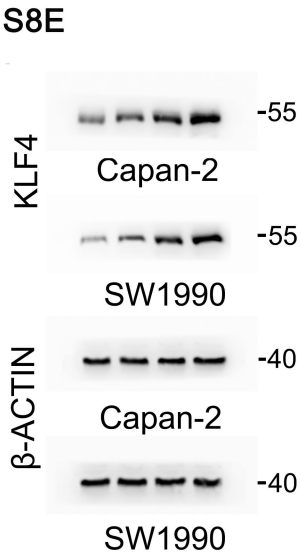

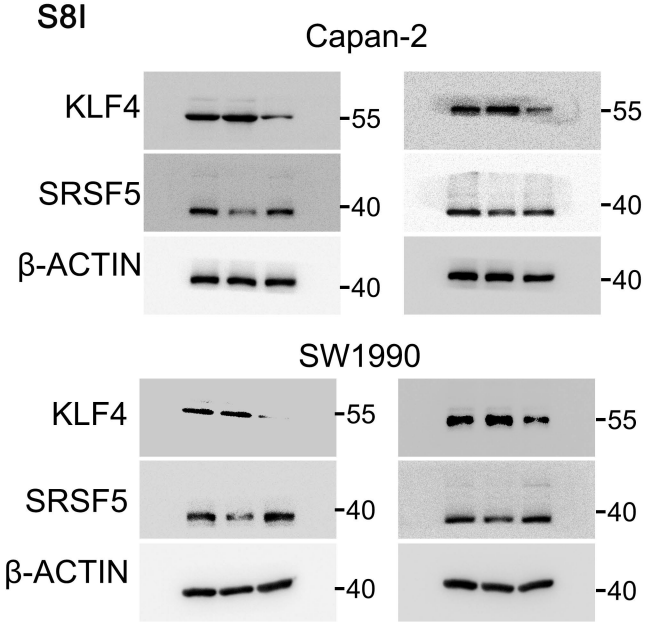

Full unedited gel for Supplementary Figure 9

S9A

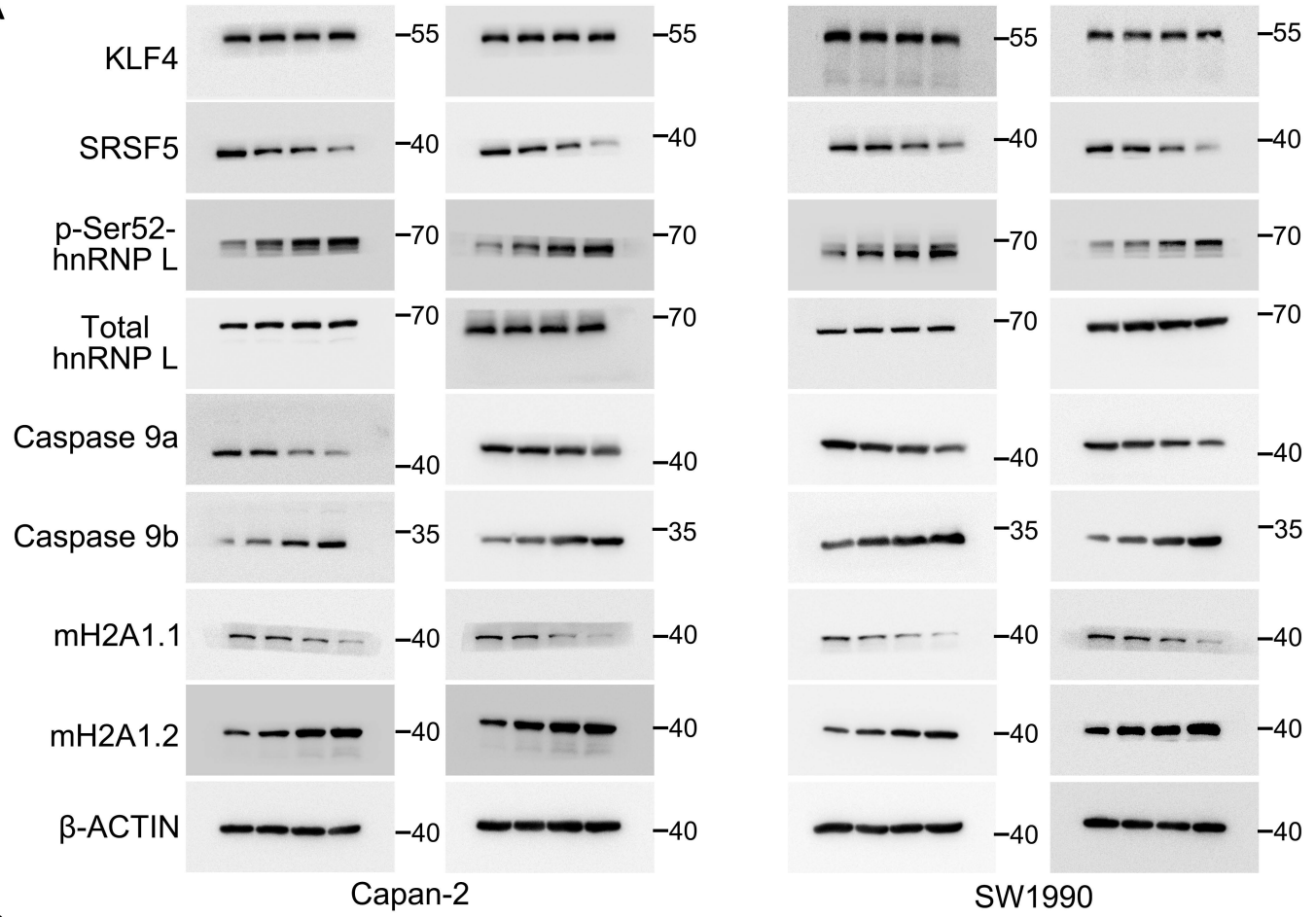

S9B

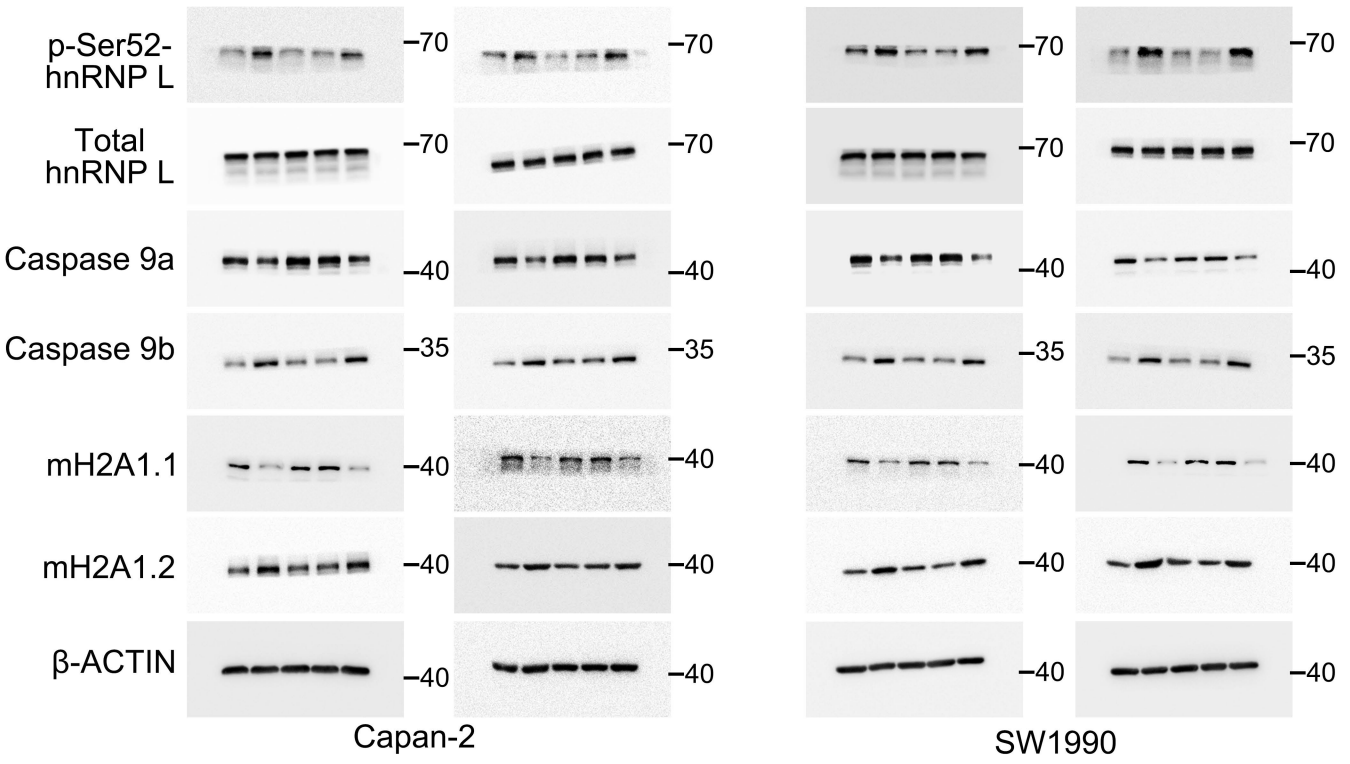

Full unedited gel for Supplementary Figure 10

S10E

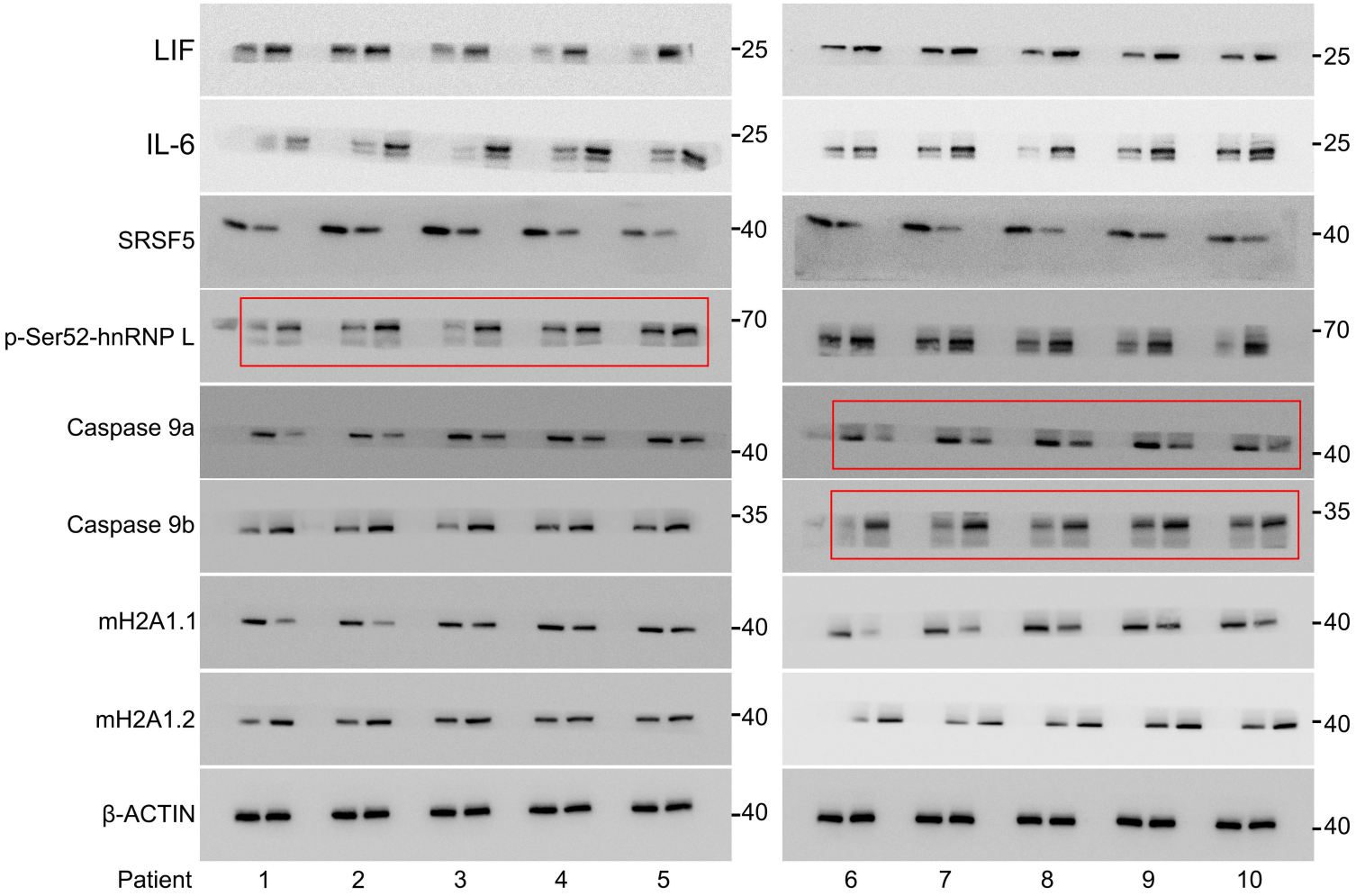

Full unedited gel for Supplementary Figure 14

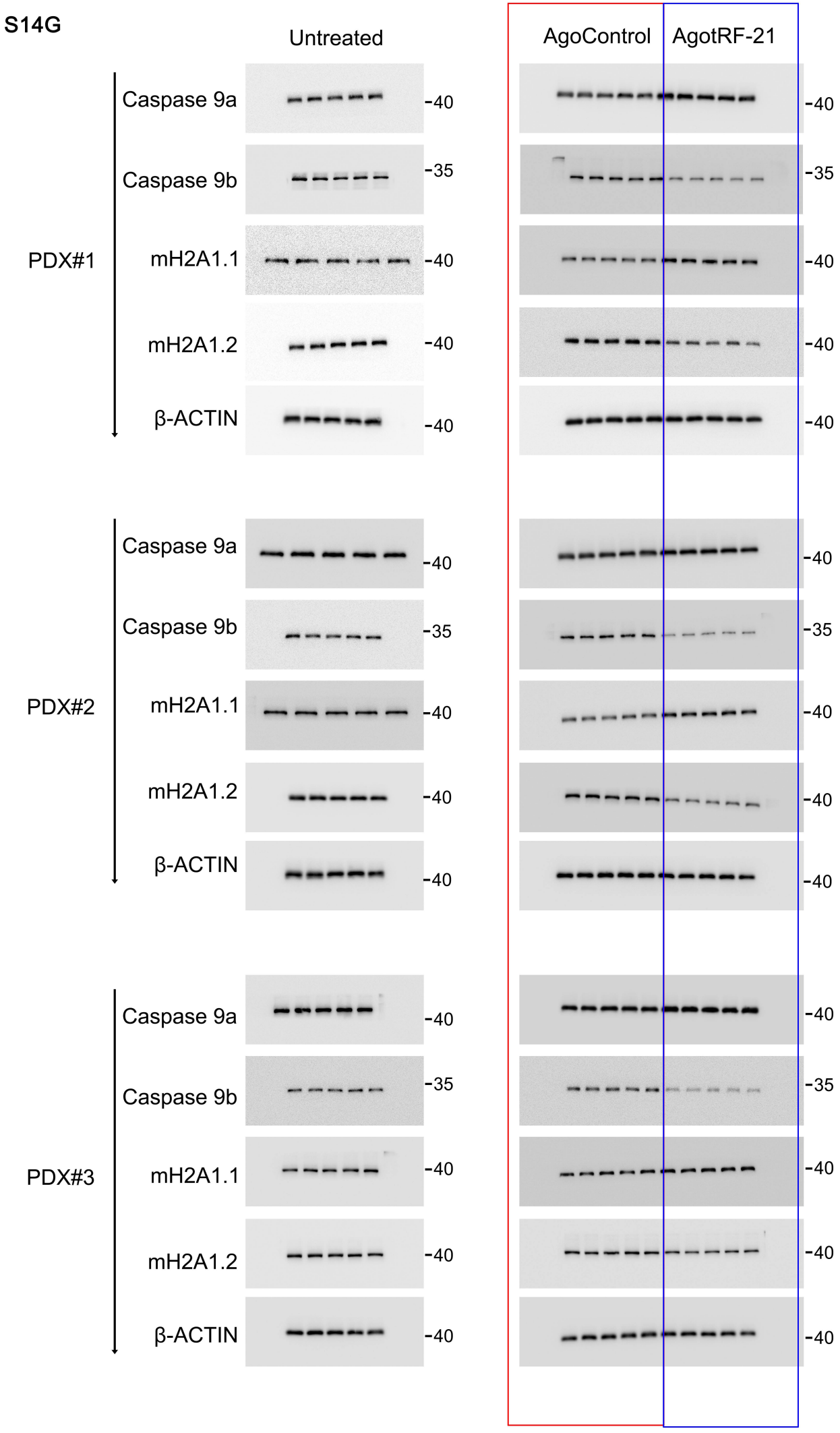

Table S1. Ten top PDAC survival associated tRFs (TCGA data).

tRF symbol	FDR	HR (95% CI)
tRF-28-Z6EXEY0VWUD2	0.035	0.43 (0.28-0.67)
tRF-18-H5KQBFD2	0.121	0.50 (0.33-0.76)
tRF-29-7O58J0K8UMII	0.156	0.51 (0.33-0.78)
tRF-21-VBY9PYKHD	0.237	0.55 (0.36-0.83)
tRF-25-5BF900BY4D	0.237	0.56 (0.37-0.86)
tRF-22-ZKXU53K8N	0.237	0.57 (0.38-0.87)
tRF-18-R29P4P04	0.237	1.73 (1.14-2.63)
tRF-17-863IP52	0.237	1.73 (1.14-2.63)
tRF-24-R959KUMKEV	0.237	1.70 (1.13-2.57)
tRF-30-RS9NS334L2H1	0.237	0.58 (0.38-0.89)

HR, hazard ratio; CI, confidence interval.

Table S2. Proteins interacted with *tRF-21-VBY9PYKHD* in PDAC cell lines identified by mass spectrometry

No.	Name and official symbol	emPAI (Capan-2)	emPAI (SW1990)
1	THO complex subunit 4, ALYREF	0.60	0.12
2	Heterogeneous nuclear ribonucleoprotein L, HNRNPL	0.49	0.73
3	Cytochrome c oxidase subunit 7A2, mitochondrial, COX7A2	0.38	0.37
4	60S acidic ribosomal protein P2, RPLP2	0.30	0.30
5	High mobility group protein B1, HMGB1	0.29	0.13
6	Histone H2B type 2-F, HIST2H2BF	0.25	0.25
7	Four and a half LIM domains protein 2, FHL2	0.22	0.10
8	Cyclin-dependent kinase 4 inhibitor D, CDKN2D	0.18	0.19
9	DNA topoisomerase 1, TOP1	0.15	0.04
10	Ras-related protein Rab-5C, RAB5C	0.14	0.14
11	Peroxiredoxin-6, PRDX6	0.13	0.13
12	Nuclear migration protein nudC, NUDC	0.09	0.09
13	Replication factor C subunit 4, RFC4	0.08	0.08
14	Translation initiation factor eIF-2B subunit beta, EIF2B2	0.08	0.08
15	Phospholipase ABHD3, ABHD3	0.07	0.07
16	Saccharopine dehydrogenase-like oxidoreductase, SCCPDH	0.07	0.07
17	CHRNA7-FAM7A fusion protein, CHRFAM7A	0.07	0.07
18	Secernin-1, SCRN1	0.07	0.07
19	B-cell lymphoma 3 protein, BCL3	0.07	0.07
20	Succinyl-CoA ligase [ADP-forming] subunit beta, mitochondrial, SUCLA2	0.07	0.07
21	Negative elongation factor A, NELFA	0.06	0.06
22	Ataxin-10, ATXN10	0.06	0.06
23	Serum albumin, ALB	0.05	0.59
24	Heterogeneous nuclear ribonucleoprotein L-like, HNRNPLL	0.05	0.24
25	Ran GTPase-activating protein 1, RANGAP1	0.05	0.05
26	Lamin-B1, LMNB1	0.05	0.05
27	A-kinase anchor protein 17A, AKAP17A	0.04	0.04
28	Crooked neck-like protein 1, CRNKL1	0.03	0.21
29	Pumilio homolog 1, PUM1	0.03	0.03
30	Oral-facial-digital syndrome 1 protein, OFD1	0.03	0.03
31	Programmed cell death 6-interacting protein, PDCD6IP	0.03	0.03
32	Tyrosine-protein kinase JAK1, JAK1	0.02	0.02
33	Non-receptor tyrosine-protein kinase TYK2, TYK2	0.02	0.02
34	Kinesin-like protein KIF13A, KIF13A	0.02	0.02
35	Sterile alpha motif domain-containing protein 9, SAMD9	0.02	0.02
36	Spectrin beta chain, non-erythrocytic 5, SPTBN5	0.01	0.01
37	Nipped-B-like protein, NIPBL	0.01	0.01
38	Serine/threonine-protein kinase mTOR, MTOR	0.01	0.01

Table S3. Proteins interacted with p-Ser52-hnRNP L identified by mass spectrometry (emPAI ≥ 0.10).

No.	Name and official symbol	Protein mass	emPAI
1	Calmodulin, CALM1	16827	31.22
2	Probable ATP-dependent RNA helicase DDX17, DDX17	81073	5.71
3	Histone H2B type 1-N, HIST1H2BN	13914	3.66
4	Heterogeneous nuclear ribonucleoprotein L, HNRNPL	64720	3.21
5	Histone H1.3, HIST1H1D	22336	1.66
6	Serine/threonine-protein phosphatase PP1-alpha catalytic subunit, PPP1CA	38229	0.94
7	Guanine nucleotide-binding protein G(I)/G(S)/G(T) subunit beta-1, GNB1	38151	0.94
8	LIM and SH3 protein 1, LASP1	19025	0.92
9	Polyadenylate-binding protein, PABPC1	58727	0.82
10	Histone H3.1t, HIST3H3	15613	0.80
11	Tubulin alpha-8 chain, TUBA8	52750	0.62
12	Mitochondrial import inner membrane translocase subunit TIM16, PAM16	5922	0.61
13	14-3-3 protein zeta/delta, YWHAZ	27899	0.57
14	Histone H2A type 1-C, HIST1H2AC	14097	0.54
15	Microtubule-associated proteins 1A/1B light chain 3A, MAP1LC3A	14320	0.53
16	Angiopoietin-like protein 8, ANGPTL8	6736	0.53
17	Guanine nucleotide-binding protein G(I)/G(S)/G(O) subunit gamma-5, GNG5	7428	0.48
18	Brain-specific angiogenesis inhibitor 1-associated protein 2, BAIAP2	16031	0.47
19	Heat shock protein HSP 90-alpha, HSP90AA1	85006	0.46
20	POTE ankyrin domain family member E, POTEE	122882	0.44
21	Malate dehydrogenase, mitochondrial, MDH2	35937	0.42
22	RNA-binding protein 39, RBM39	26853	0.42
23	tRNA dimethylallyltransferase, mitochondrial, TRIT1	8437	0.42
24	MICOS complex subunit, CHCHD3	27832	0.40
25	Serine/threonine-protein kinase DCLK2, DCLK2	8739	0.40
26	ATP-dependent RNA helicase DDX3X, DDX3X	82110	0.37

27	Cilia- and flagella-associated protein 57, CFAP57	9437	0.37
28	Ras-related protein Rap-1A, RAP1A	21316	0.34
29	MICOS complex subunit MIC60, IMMT	68305	0.33
30	Core-binding factor subunit beta, CBFB	21723	0.33
31	Dynein light chain 1, cytoplasmic, DYNLL1	10530	0.33
32	Histone H1x, H1FX	22474	0.32
33	Kynurenine formamidase, AFMID	10760	0.32
34	Annexin A5, ANXA5	35971	0.30
35	Elongation factor 1-beta, EEF1B2	24919	0.29
36	Transcription factor BTF3, BTF3	11795	0.29
37	L-lactate dehydrogenase A chain, LDHA	36950	0.29
38	Cytochrome c, CYCS	11855	0.29
39	Zinc finger protein 582, ZNF582	11713	0.29
40	Transmembrane protein 213, TMEM213	11855	0.29
41	Dystrobrevin alpha, DTNA	12405	0.28
42	Heterogeneous nuclear ribonucleoprotein R, HNRNPR	55912	0.26
43	THO complex subunit 4, ALYREF	26872	0.26
44	Hepatoma-derived growth factor, HDGF	26886	0.26
45	D-3-phosphoglycerate dehydrogenase, PHGDH	57356	0.25
46	Tyrosine-protein kinase, HCK	59986	0.24
47	Prohibitin, PHB	29843	0.24
48	Signal recognition particle 14 kDa protein, SRP14	14675	0.23
49	D-beta-hydroxybutyrate dehydrogenase, mitochondrial, BDH1	14843	0.23
50	Complement component 1 Q subcomponent-binding protein, mitochondrial, C1QBP	31742	0.22
51	Histone-binding protein RBBP4, RBBP4	47911	0.22
52	DNA-directed RNA polymerases I, II, and III subunit RPABC1, POLR2E	15579	0.22
53	Polyadenylate-binding protein, PABPC4	68156	0.21
54	Transformer-2 protein homolog beta, TRA2B	33760	0.21
55	Transcriptional activator protein Pur-beta, PURB	33392	0.21

56	Eukaryotic translation initiation factor 5A, EIF5A	16336	0.21
57	Stathmin, STMN1	17292	0.20
58	Ras GTPase-activating protein-binding protein 2, G3BP2	54145	0.19
59	Serine hydroxymethyltransferase, mitochondrial, SHMT2	56414	0.19
60	Cytochrome c oxidase subunit 5A, mitochondrial, COX5A	17452	0.19
61	tRNA (adenine(37)-N6)-methyltransferase, TRMO	17746	0.19
62	Procollagen-lysine,2-oxoglutarate 5-dioxygenase 3, PLOD3	19206	0.18
63	Sterile alpha motif domain-containing protein 12, SAMD12	18355	0.18
64	Neurexin-3-beta, NRXN3	19069	0.18
65	Proteasome activator complex subunit 3, PSME3	19864	0.17
66	Protein Dr1, DR1	19660	0.17
67	Acidic leucine-rich nuclear phosphoprotein 32 family member A, ANP32A	20099	0.17
68	ES1 protein homolog, mitochondrial, C21orf33	20566	0.16
69	Proteasome subunit alpha type-7, PSMA7	21315	0.16
70	Casein kinase II subunit alpha 3, CSNK2A3	45305	0.15
71	Cerebellin-4, CBLN4	21908	0.15
72	DPY30 domain-containing protein 2, DYDC2	22381	0.15
73	SRSF protein kinase 3, SRPK3	22691	0.15
74	Adenosylhomocysteinase, AHCY	48255	0.14
75	Osteoclast-stimulating factor 1, OSTF1	23943	0.14
76	Small nuclear ribonucleoprotein-associated proteins B and B', SNRPB	24765	0.14
77	Peptidyl-prolyl cis-trans isomerase B, PPIB	23785	0.14
78	DNA replication complex GINS protein PSF3, GINS3	24576	0.14
79	Transmembrane emp24 domain-containing protein 10, TMED10	25131	0.13
80	RNA-binding protein FUS, FUS	53622	0.13
81	Transcription factor A, mitochondrial, TFAM	26004	0.13
82	Proteasome subunit alpha type-4, PSMA4	26494	0.13
83	Protein Mis18-beta, OIP5	25189	0.13
84	Glucose-induced degradation protein 8 homolog, GID8	26789	0.12

85	mRNA turnover protein 4 homolog, MRTO4	27657	0.12
86	Coronin-1B, CORO1B	54885	0.12
87	GTP-binding nuclear protein Ran, RAN	27027	0.12
88	UPF0568 protein C14orf166, C14orf166	28165	0.12
89	Serine/arginine-rich splicing factor 7, SRSF7	27578	0.12
90	Nucleolar protein 16, NOP16	27079	0.12
91	3-hydroxyacyl-CoA dehydrogenase type-2, HSD17B10	27134	0.12
92	Protein phosphatase 1G, PPM1G	59919	0.11
93	T-complex protein 1 subunit theta, CCT8	60153	0.11
94	Heterogeneous nuclear ribonucleoprotein H, HNRNPH1	30590	0.11
95	Voltage-dependent anion-selective channel protein 2, VDAC2	30842	0.11
96	Polypyrimidine tract-binding protein 1, PTBP1	62653	0.11
97	Proliferating cell nuclear antigen, PCNA	29092	0.11
98	PMS1 protein homolog 1, PMS1	31209	0.11
99	Gelsolin, GSN	29107	0.11
100	Mitochondrial uncoupling protein 2, UCP2	30849	0.11
101	Outer dense fiber protein 3-like protein 2, ODF3L2	31218	0.11
102	Serine/arginine-rich splicing factor 8, SRSF8	32382	0.10
103	WD repeat-containing protein 1, WDR1	66836	0.10
104	GTP-binding protein RAD, RRAD	33453	0.10
105	DNA repair protein complementing XP-A cells, XPA	31747	0.10
106	V-type proton ATPase subunit a, TCIRG1	33055	0.10
107	Putative SCAN domain-containing protein SCAND2P, SCAND2P	34652	0.10

Table S4. RNA binding proteins predicted by RBPmap that might interact with *tRNA*^{GlyGCC}.

Protein	*Z*-score	*P*-value
hnRNP A2B1	1.677	4.68×10^{-2}
hnRNP F	2.787	2.66×10^{-3}
hnRNP M	2.984	1.42×10^{-3}
MBNL1	2.088	1.84×10^{-2}
RBM4	2.681	3.67×10^{-3}
SRSF3	2.020	2.17×10^{-2}
SRSF5	2.516	5.93×10^{-3}
TRA2B	1.726	4.22×10^{-2}

Table S5. Baseline demographic and clinical characteristics of individuals with pancreatic ductal adenocarcinoma (PDAC) in this study

	Cohort 1		Cohort 2		Pooled samples	
	Alive (*n* = 36)	Deceased (*n* = 122)	Alive (*n* = 13)	Deceased (*n* = 56)	Alive (*n* = 49)	Deceased (*n* = 178)
Age, mean (SEM[a])	59.8 (2.0)	61.1 (1.0)	60.1(1.9)	63.1 (1.5)	59.9 (1.5)	61.7 (0.8)
Sex, *n* (%)						
Male	23 (63.9)	68 (55.7)	6 (46.2)	35 (62.5)	29 (59.2)	103 (57.9)
Female	13 (36.1)	54 (44.3)	7 (53.8)	21 (37.5)	20 (40.8)	75 (42.1)
Differentiation, *n* (%)						
Well	7 (19.4)	13 (10.7)	3 (23.1)	6 (10.7)	10 (20.4)	19 (10.7)
Moderate	22 (61.2)	81 (66.4)	8 (61.5)	31 (55.4)	30 (61.2)	112 (62.9)
Poor	7 (19.4)	28 (22.9)	2 (15.4)	19 (33.9)	9 (18.4)	47 (26.4)
Lymph node metastasis, *n* (						
Positive	14 (38.9)	66 (54.1)	7 (53.8)	27 (48.2)	21 (42.9)	93 (52.2)
Negative	22 (61.1)	56 (45.9)	6 (46.2)	29 (51.8)	28 (57.1)	85 (47.8)
Vascular invasion, *n* (%)						
Yes	10 (27.8)	39 (32.0)	5 (38.5)	27 (48.2)	15 (30.6)	66 (37.1)
No	26 (72.2)	83 (68.0)	8 (61.5)	29 (51.8)	34 (69.4)	112 (62.9)
Neural invasion, *n* (%)						
Yes	23 (63.9)	74 (60.7)	3 (23.1)	10 (17.9)	26 (53.1)	84 (47.2)
No	13 (36.1)	48 (39.3)	10 (76.9)	46 (82.1)	23 (46.9)	94 (52.8)
TNM stage[b], *n* (%)						
I	1 (2.8)	6 (4.9)	3 (23.1)	9 (16.0)	4 (8.2)	15 (8.4)
II	29 (80.6)	100 (82.0)	8 (61.5)	27 (48.2)	37 (75.5)	127 (71.3)
III	0 (0.0)	4 (3.3)	2 (15.4)	10 (17.9)	2 (4.1)	14 (7.9)
IV	6 (16.7)	12 (9.8)	0 (0.0)	10 (17.9)	6 (12.2)	22 (12.4)
Smoking status, *n* (%)						
Ever	8 (22.2)	44 (36.1)	3 (23.1)	18 (32.1)	11 (22.4)	62 (34.8)
Never	28 (77.8)	78 (63.9)	10 (76.9)	38 (67.9)	38 (77.6)	116 (65.2)
Drinking status, *n* (%)						
Ever	5 (13.9)	21 (17.2)	4 (30.8)	16 (28.6)	9 (18.4)	37 (20.8)
Never	31 (86.1)	101 (82.8)	9 (69.2)	40 (71.4)	40 (81.6)	141 (79.2)
Treatment, *n* (%)						

Surgery only	13 (36.1)	69 (56.6)	6 (46.2)	26 (46.4)	19 (38.8)	95 (53.4)
Surgery + chemotherapy	23 (63.9)	53 (43.4)	7 (53.8)	30 (53.6)	30 (61.2)	83 (46.6)

[a]SEM, standard error of mean.

[b]Tumor TNM staging were reviewed by at least 3 pathologists and defined according to the American Joint Committee on Cancer (AJCC) 8th edition.

Table S6. Sequences of siRNAs or mimics used in this study.

siRNAs	Sequence (5’ → 3’)
siControl	UUCUCCGAACGUGUCACGUTT
siHNRNPL#1	CACUGGUGGAGUUUGAAGATT
siHNRNPL#2	CCCAUUUAUUCGAUCACCATT
siDDX17#1	CCUUCCAUCAUGCUAACUUTT
siDDX17#2	GCUGACAGAAUGCUUGAUATT
siHNRNPA2B1#1	GCGGAAUUAAAGAAGAUACTT
siHNRNPA2B1#2	GGACCAGGAAGUAACUUUATT
siHNRNPF#1	CCGCAGGUGUCCAUUUCAUTT
siHNRNPF#2	GGUACAUUGAGGUGUUCAATT
siHNRNPM#1	GGCAUAGGAUUUGGAAUAATT
siHNRNPM#2	GAGCCUUCAUUACAAACAUTT
siRBM4#1	GCAAACGAAUGCACGUGCATT
siRBM4#2	GGUCCAAAGAGUGUCCGAUTT
siSRSF3#1	CAUCGUGAUUCCUGUCCAUTT
siSRSF3#2	GCUAGAUGGAAGAACACUATT
siSRSF5#1	GGAUCCAAGGGAUGCAGAUTT
siSRSF5#2	GCACACCGACCUAAAUUAATT
siMBNL1#1	CCAGACACGGAAUGUAAAUTT
siMBNL1#2	GCCUGGUCCCGGCAGAGAUTT
siTRA2B#1	GGUCUUACAGUCGAGAUUATT
siTRA2B#2	CCCAUUGCCGAUGUGUCUATT
siKLF4#1	CCGAGGAGUUCAACGAUCUTT
siKLF4#2	CCUUACACAUGAAGAGGCATT
siKRAS#1	GCGUAGGCAAGAGUGCCUUTT
siKRAS#2	GGACUUAGCAAGAAGUUAUTT
siAKT2#1	GGGCUAAAGUGACCAUGAATT
siAKT2#2	GGUACUUCGAUGAUGAAUUTT
siAKT1#1	AGGAAGUCAUCGUGGCCAATT
siAKT1#2	GCACUUUCGGCAAGGUGAUTT
Mimics	Sequence (5’→ 3’)
tRF-21-VBY9PYKHD Control	UUGUACUACACAAAAGUACUG
tRF-21-VBY9PYKHD mimics	UAGAAUUCUCGCCUGCCACGC
agoControl	UUCUCCGAACGUGUCACGUTT
agotRF-21-VBY9PYKHD	UAGAAUUCUCGCCUGCCACGC

Table S7. Primers, probes and adaptor used in this study

Northern blot (DIG-labeled)	Sequence (5’ → 3’)
tRF-21-VBY9PYKHD probe	GCGUGGCAGGCGAGAAUUCUA
FL-PCR	Sequence (5’ → 3’)
TaqMan probe	5’-/56-FAM/CCATCGTAG/ZEN/GGTCCGAGGTATTC/3IABkFQ/-3’
SL-adaptor-U	/5Phos/TCGTAGGGTCCGAGGTATTCACGATGrGrU
tRNA^{GlyGCC} -F primer	CGGGAGGCCCGGGTTCGATT
tRNA^{GlyGCC} -R/RT primer	CGAGAATTCTACCACTGAACCACCAATGC
5S rRNA-F primer	TACGGCCATACCACCCTGAAC
5S rRNA-R primer	CGGTCTCCCATCCAAGTACTAACC
Primers for alternative splicing	Sequence (5’ → 3’)
Caspase 9-F	GCTCTTCCTTTGTTCATCTCC
Caspase 9-R	CATCTGGCTCGGGGTTACTGC
macroH2A1.1-F	ACTGACTTCTACATCGGTGG
macroH2A1.2-F	TCCTTGGCCAGAAGCTGAAC
macroH2A1E8-R	GAGTTCCAGGACAGCTTCCAC
RNA pull down probes (3’-biotin)	Sequence (5’ → 3’)
non-targeting oligo	UUGUACUACACAAAAGUACUG
tRF-21-VBY9PYKHD sense	UAGAAUUCUCGCCUGCCACGC
tRF-21-VBY9PYKHD antisense	GCGUGGCAGGCGAGAAUUCUA

RNA sequences for *In vitro* kinase assay	Sequence (5’ → 3’)
tRF-21-VBY9PYKHD sense	UAGAAUUCUCGCCUGCCACGC
tRF-21-VBY9PYKHD antisense	GCGUGGCAGGCGAGAAUUCUA

Reverse transcription primers for tRFs	Sequence (5’ → 3’)
tRF-21-VBY9PYKHD	GTCGTATCCAGTGCGTGTCGTGGAGTCGGCAATTGCACTGGATACGACGCGTGGCA
tRF-28-Z6EXEY0VWUD2	GTCGTATCCAGTGCGTGTCGTGGAGTCGGCAATTGCACTGGATACGACTGGTCAGA
tRF-18-H5KQBFD2	GTCGTATCCAGTGCGTGTCGTGGAGTCGGCAATTGCACTGGATACGACTGGTGTTT
tRF-29-7O58J0K8UMII	GTCGTATCCAGTGCGTGTCGTGGAGTCGGCAATTGCACTGGATACGACATGCGATT
tRF-25-5BF900BY4D	GTCGTATCCAGTGCGTGTCGTGGAGTCGGCAATTGCACTGGATACGACGTTAGCAG
tRF-22-ZKXU53K8N	GTCGTATCCAGTGCGTGTCGTGGAGTCGGCAATTGCACTGGATACGACACCCGGGA
tRF-18-R29P4P04	GTCGTATCCAGTGCGTGTCGTGGAGTCGGCAATTGCACTGGATACGACCCACTGAG
tRF-17-863IP52	GTCGTATCCAGTGCGTGTCGTGGAGTCGGCAATTGCACTGGATACGACTGGTGGCA
tRF-24-R959KUMKEV	GTCGTATCCAGTGCGTGTCGTGGAGTCGGCAATTGCACTGGATACGACGGCTCCCC
tRF-30-RS9NS334L2H1	GTCGTATCCAGTGCGTGTCGTGGAGTCGGCAATTGCACTGGATACGACGGTATTCT

qRT-PCR primers for tRFs	Sequence (5’ → 3’)	
	Forward	Reverse
tRF-21-VBY9PYKHD	GAATTCTCGCCTGCCACG	CAGTGCGTGTCGTGGAGT
tRF-28-Z6EXEY0VWUD2	TGACCGCTCTGACCAGT	CAGTGCGTGTCGTGGAGT
tRF-18-H5KQBFD2	ACCCCATAAACACCAGTCGT	CAGTGCGTGTCGTGGAGT
tRF-29-7O58J0K8UMII	GCAGAGCCCGGTAATC	CAGTGCGTGTCGTGGAGT

tRF-25-5BF900BY4D	CACAAGAACTGCTAACGTCGT	CAGTGCGTGTCGTGGAGT
tRF-22-ZKXU53K8N	TTGGGTGCGAGAGGTCC	CAGTGCGTGTCGTGGAGT
tRF-18-R29P4P04	GATGTAGCTCAGTGGGTCGT	CAGTGCGTGTCGTGGAGT
tRF-17-863IP52	GCCACCAGTCGTATCCAGT	CAGTGCGTGTCGTGGAGT
tRF-24-R959KUMKEV	CGGGGAGCCGTCGTAT	CAGTGCGTGTCGTGGAGT
tRF-30-RS9NS334L2H1	TGGTTGTAGTCCGTGCGA	CAGTGCGTGTCGTGGAGT
U6	CTCGCTTCGGCAGCACA	AACGCTTCACGAATTTGCGT

Gene Symbol	Sequence (5’ → 3’)	
	Forward	Reverse
HNRNPL	TACGCAGCCGACAACCAAATA	CTCCGGGAGTCATCCGAGT
DDX17	GATGTTTGTCCTAAACCCGTGT	CCAACGGAAATCCCTGGCA
HNRNPA2B1	TGGAGGTAGCCCCGGTTATG	GGACCGTAGTTAGAAGGTTGCT
HNRNPF	GAAGGCTCTAGGGAAACACAAG	CACGGACATGAACTTCAGAGG
HNRNPM	GCGGCGACGGAGATCAAAA	CTCATTCTGAGCAGGTCGTTC
RBM4	AGAGTGTCCGATAGATCGTTCA	GAATCCCCATAGCTCATGGTG
SRSF3	TGGCAACAAGACGGAATTGGA	CAAAGCCGGGTGGGTTTCTA
SRSF5	TCTTCAAGGGATATGGACGGAT	GACCGAGCCCTAGCATGTTC
MBNL1	GCTGTTAGTGTCACACCAATTCG	AGGCGATTACTCGTCCATTTTC
TRA2B	GCGTCATGTTGGGAATCGG	CTTGAACGCCTAGACTGCTGG
KLF4	CAGCTTCACCTATCCGATCCG	GACTCCCTGCCATAGAGGAGG

LIF	ACAGAGCCTTTGCGTGAAAC	TGGTCCACACCAGCAGATAA
IL6	ACTCACCTCTTCAGAACGAATTG	CCATCTTTGGAAGGTTCAGGTTG
GAPDH	TTGGCCAGGGGTGCTAAG	AGCCAAAAGGGTCATCATCTC
ACTB	CAGGGCGTGATGGTGGGCATG	GTAGAAGGTGTGGTGCCAGATT

ChIP-qPCR	Sequence (5’ → 3’)	
	Forward	Reverse
SRSF5 promoter	CCTTGGATTTGTGGTCTCGGC	CTCCTCATTCGACACTAGATGGC

Primers for *in vitro* transcription	Sequence (5’ → 3’)	
	Forward	Reverse
tRNA^{GlyGCC}	TAATACGACTCACTATAGGGGCATTGGTGGT	TGCATTGGCCGGGAATCGAA

Table S8. Antibodies used in this study

Protein name	Host species	Product number
hnRNP L	M	Abcam, ab6106
COX7A2	R	Abcam, ab131143
RPLP2	R	Absin, abs111925
HIST2H2BF	R	Absin, abs130597
p19	M	Santa Cruz Biotechnology, sc-1665
RAB5C	M	Santa Cruz Biotechnology, sc-365667
HMGB1	R	Proteintech, 10829-1-AP
FLAG	M	Sigma, F1804
HA	M	Sigma, SAB2702196
AKT2	M	Abcam, ab175354
p-Ser474-AKT2	R	Abcam, ab38513
AKT1	R	Abcam, ab235958
KRAS	R	Abcam, ab275876
Histone H3	R	Abcam, ab1791
GAPDH	R	Cell Signaling Technology, #5174
β-ACTIN	M	Abcam, ab8226
CALM1	M	Novus Biologicals, NBP1-04268
DDX17	R	Proteintech, 19910-1-AP
HIST1H2BN	M	CreativeDiagnostics, DPAB-DC3410
HIST1H1D	R	Creative Diagnostics, DCABH-7739
PPP1A	M	Novus Biologicals, NBP1-51600
GNB1	R	Novus Biologicals, NBP1-55307
LASP1	G	Abcam, ab1301
PABP1	M	Novus Biologicals, NB120-6125
HIST3H3	M	Novus Biologicals, NBP2-52482
mH2A1	R	Cell Signaling Technology, #8551
mH2A1.1	R	Cell Signaling Technology, #12455
mH2A1.2	R	Cell Signaling Technology, #4827
SRSF5 (WB)	M	Abcam, ab67175
SRSF5 (IP)	R	Sigma-Aldrich, 06-1365
KLF4	G	R&D SYSTEMS, AF3640
RBM4	M	Santa Cruz Biotechnology, sc-373852
MBNL1	R	Novus Biologicals, NBP2-19445
Human LIF Antibody	G	R&D SYSTEMS, AF-250-NA
Human IL-6 Antibody	G	R&D SYSTEMS, AF-206-NA
LIF	R	Abcam, ab113262
IL-6	R	Abcam, ab6672

STAT3	M	Cell Signaling Technology, #9139
p-Tyr705-STAT3	R	Cell Signaling Technology, #9145
Ki67	R	ZSGB-BIO, ZA-0502
p-Ser52-hnRNP L	R	GenScript, custom-made
Caspase 9a/b	R	GenScript, custom-made

M, Mouse; R, Rabbit; G, Goat

Full unedited gel for Figure 3

3B

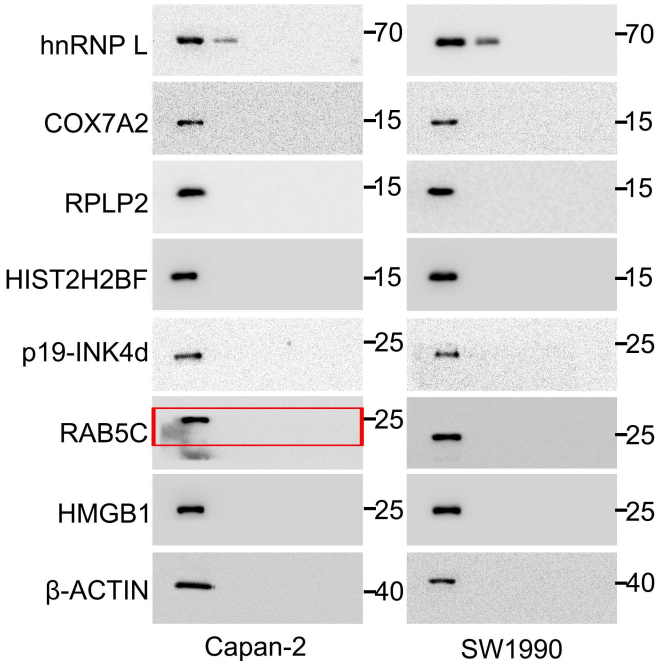

3C

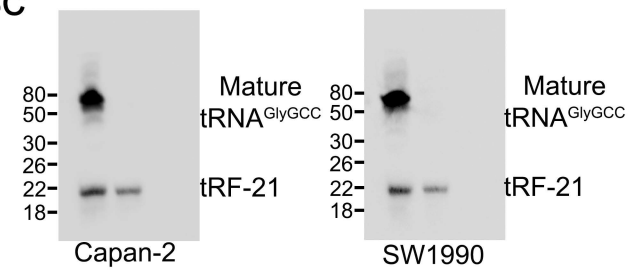

3D

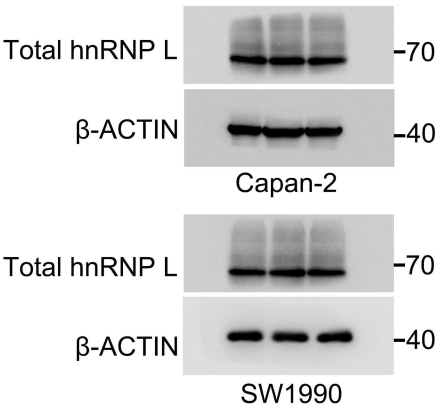

3E

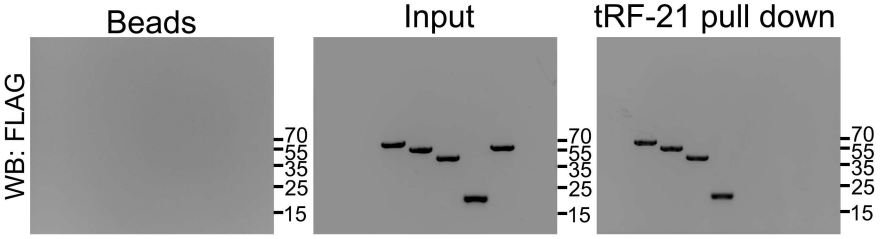

3G

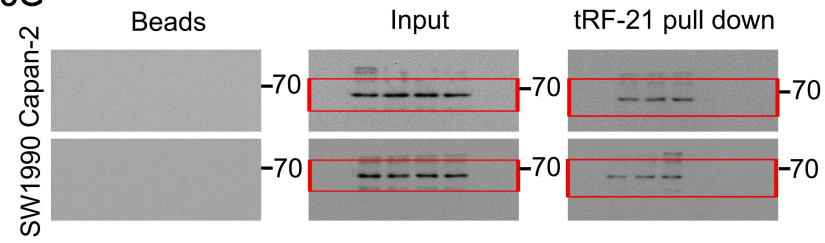

Full unedited gel for Figure 4

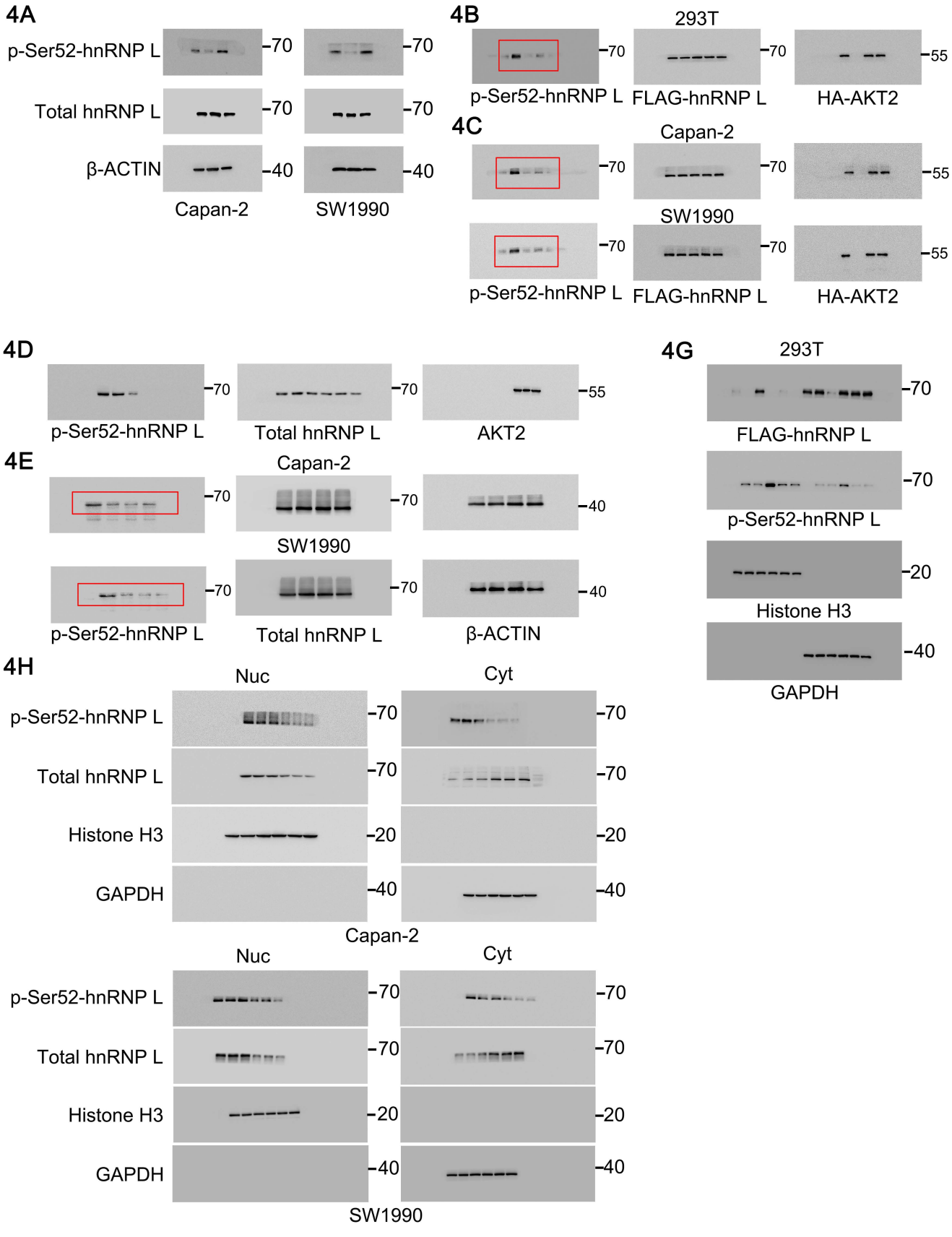

Full unedited gel for Figure 5

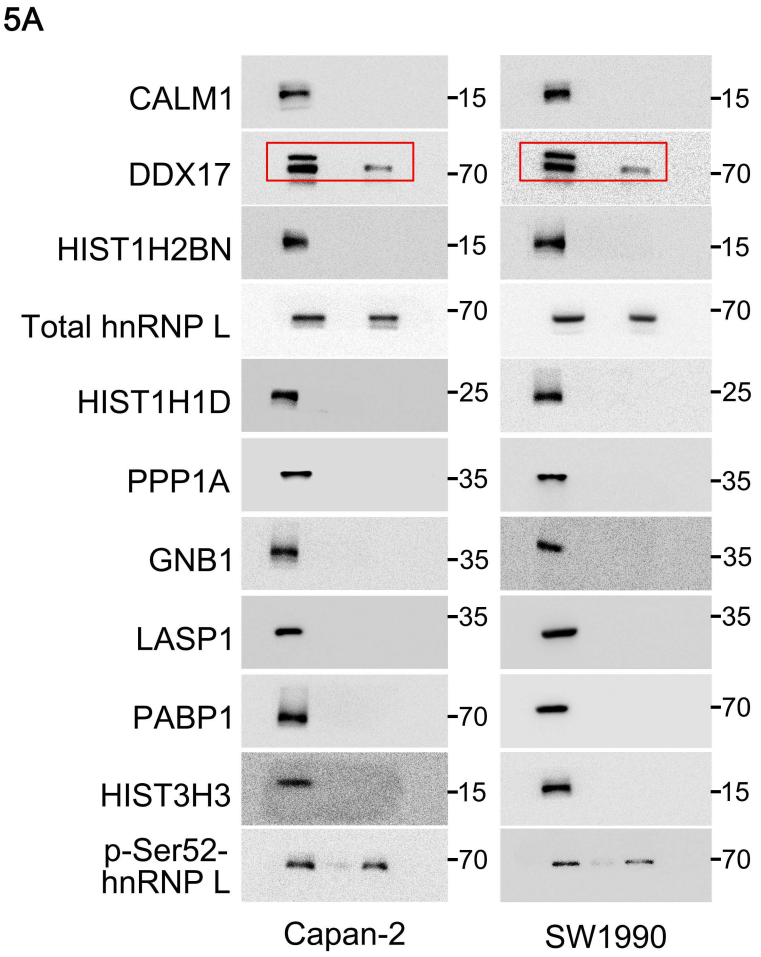

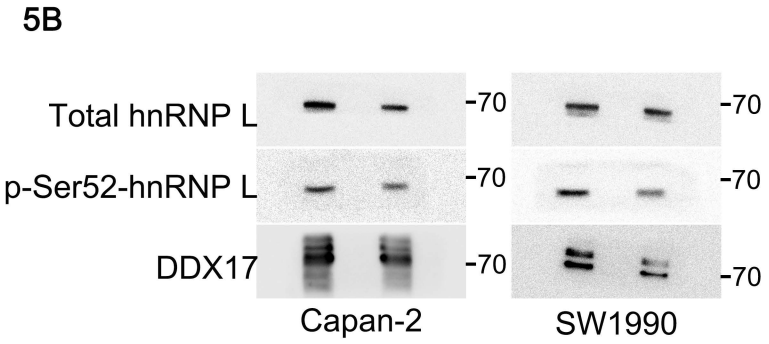

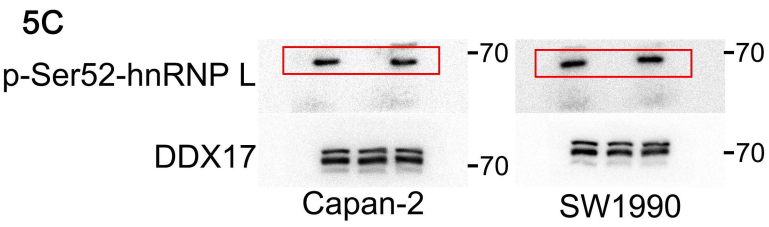

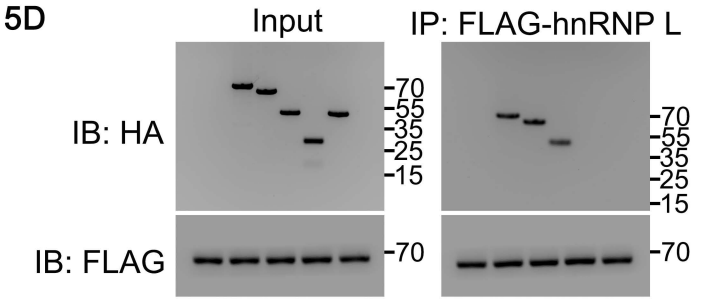

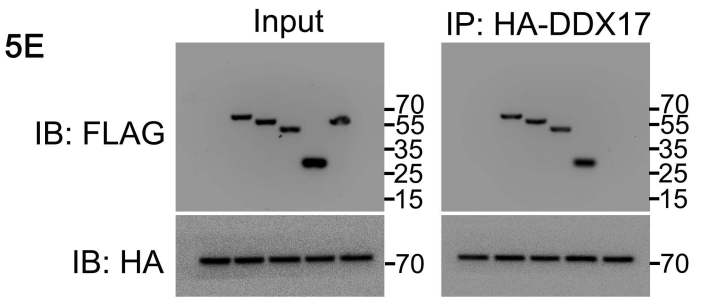

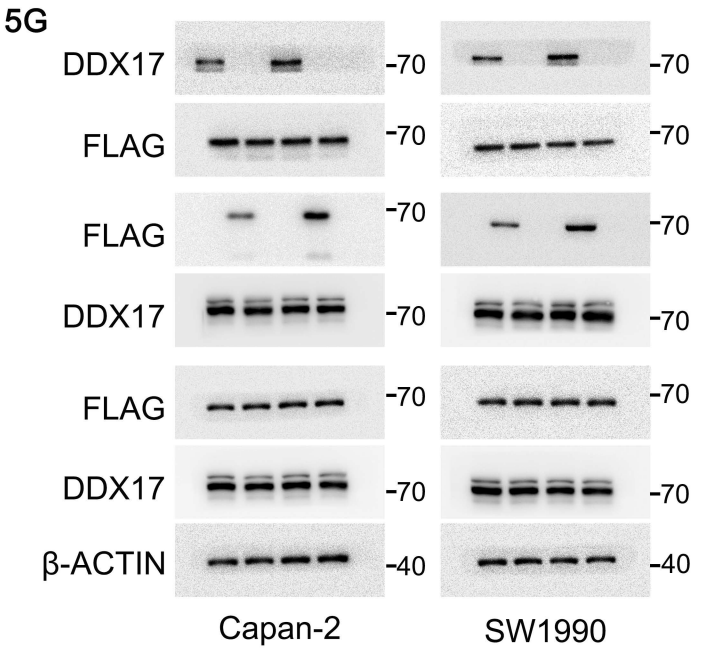

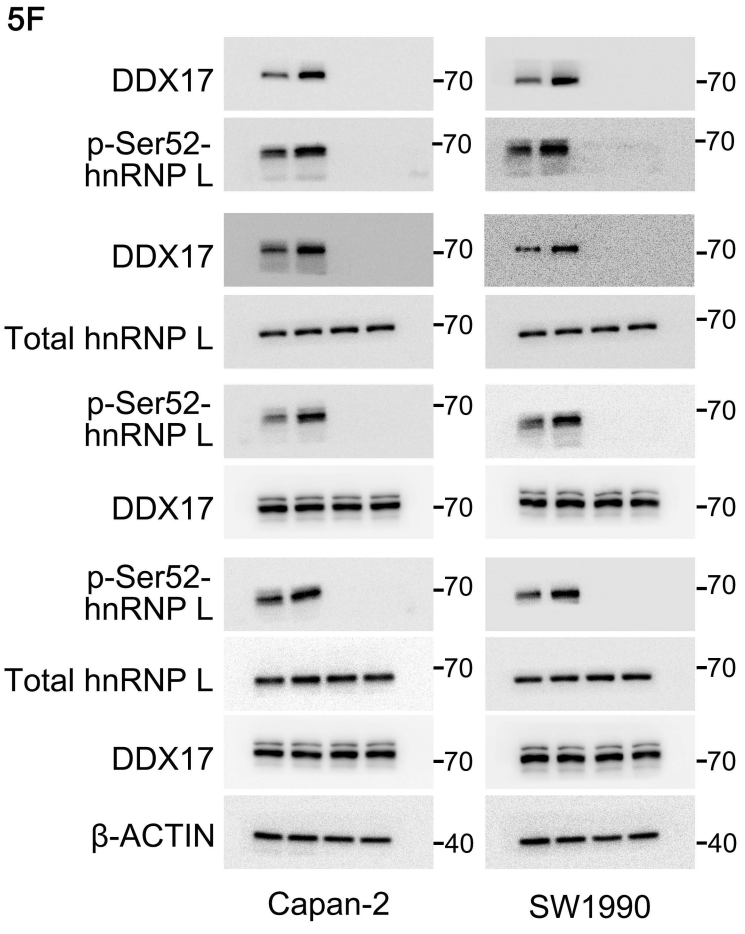

Full unedited gel for Figure 6

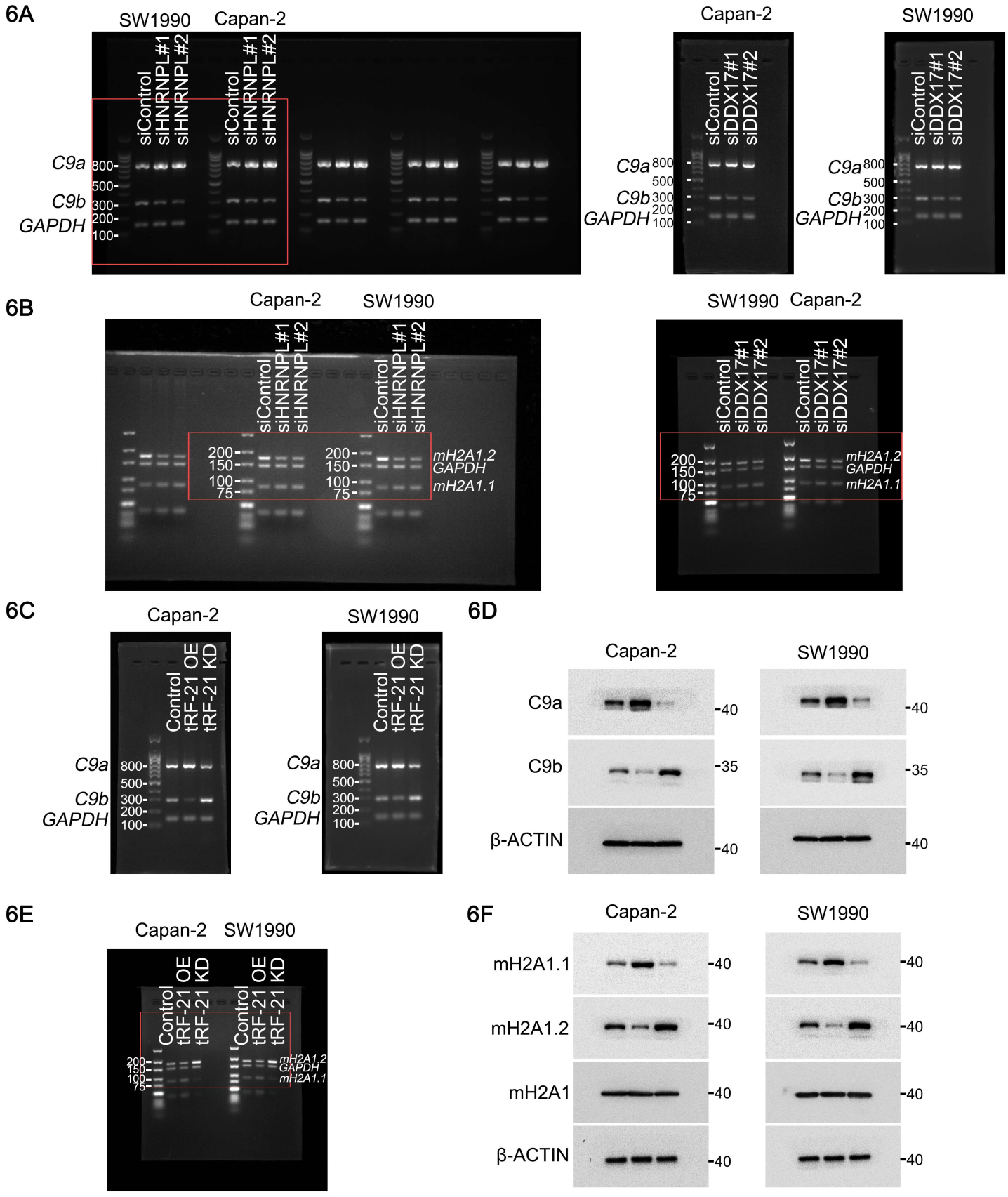

Full unedited gel for Figures 7 and 8

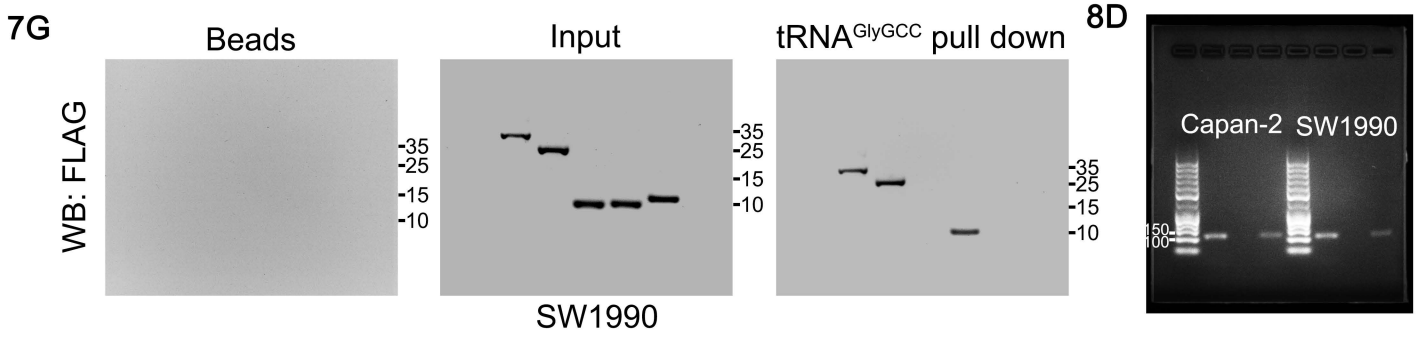

Full unedited gel for Supplementary Figures 1-5

S1D

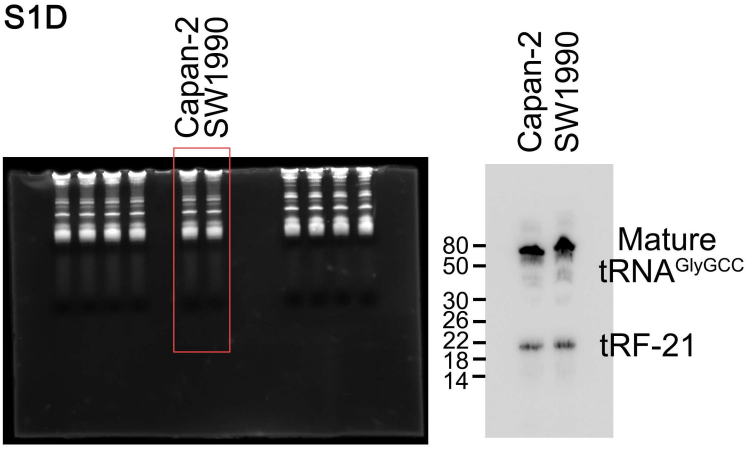

S2C

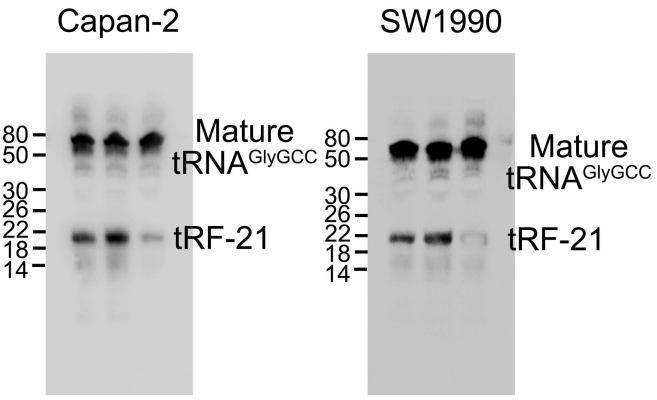

S4A

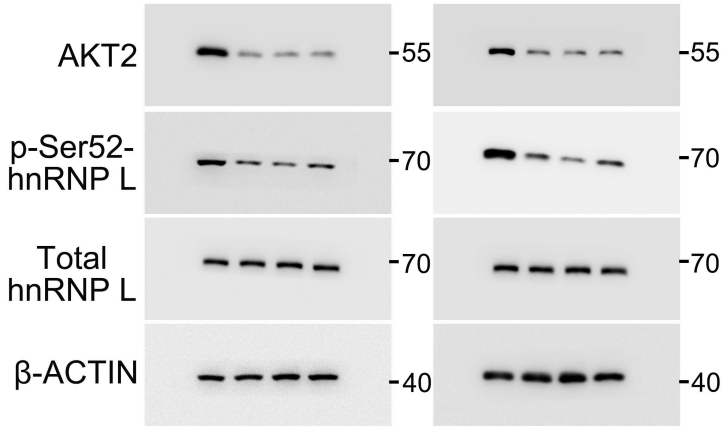

S4B

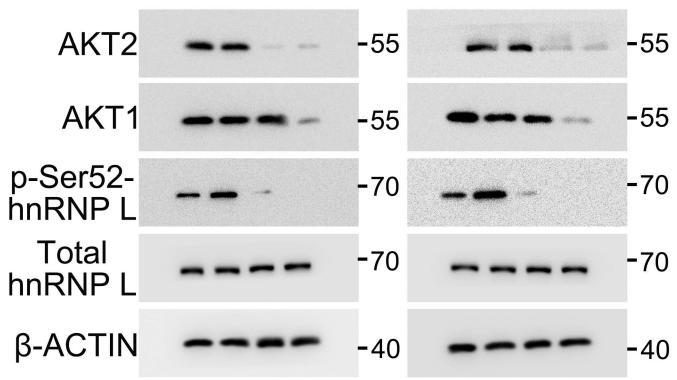

S5H

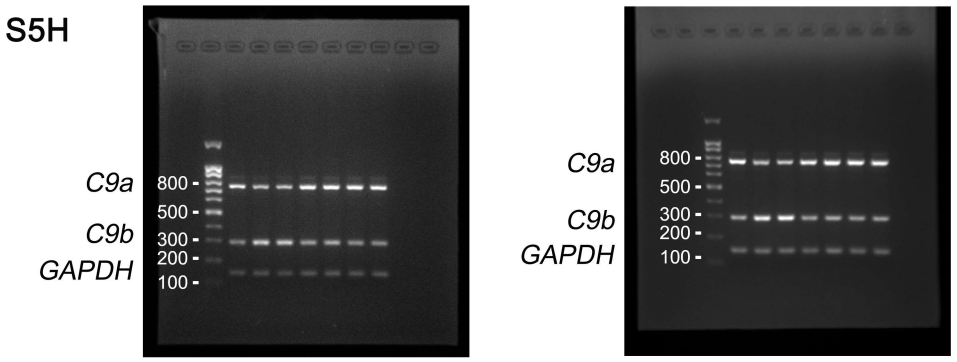

S5I

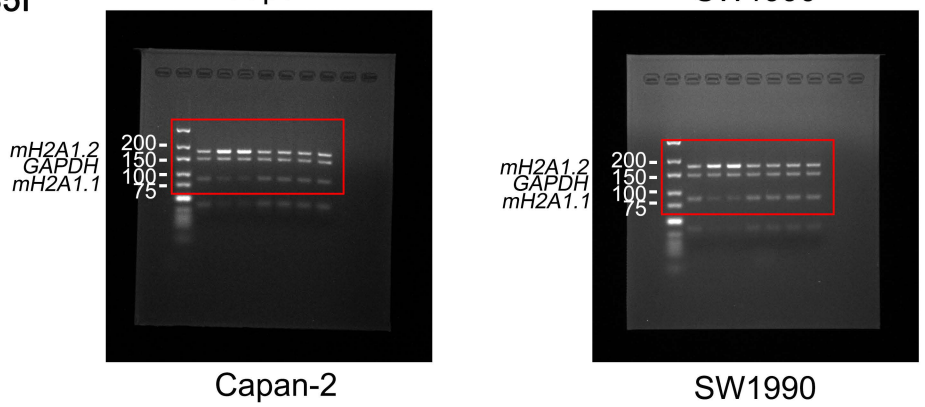

Full unedited gel for Supplementary Figures 6 and 8

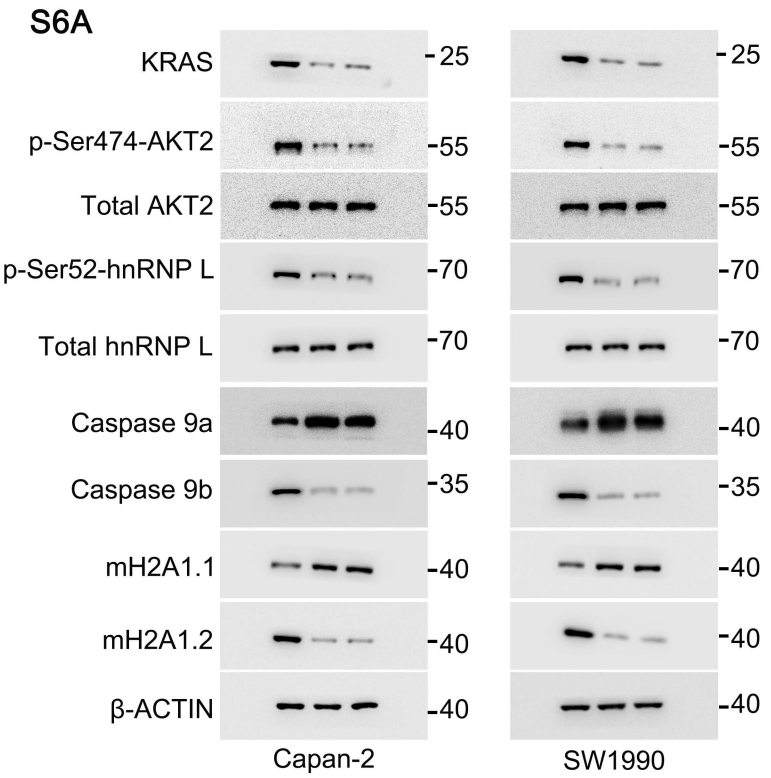

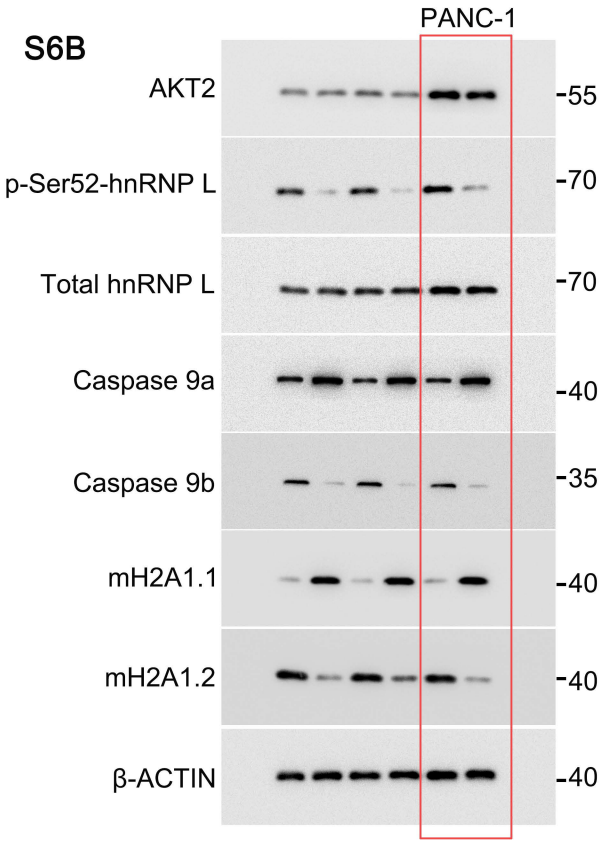

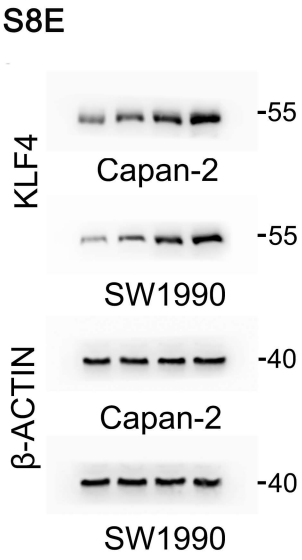

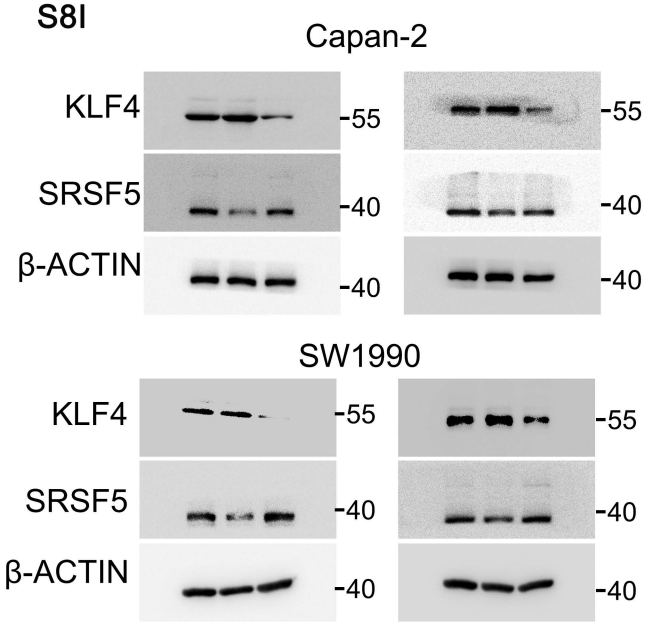

Full unedited gel for Supplementary Figure 9

S9A

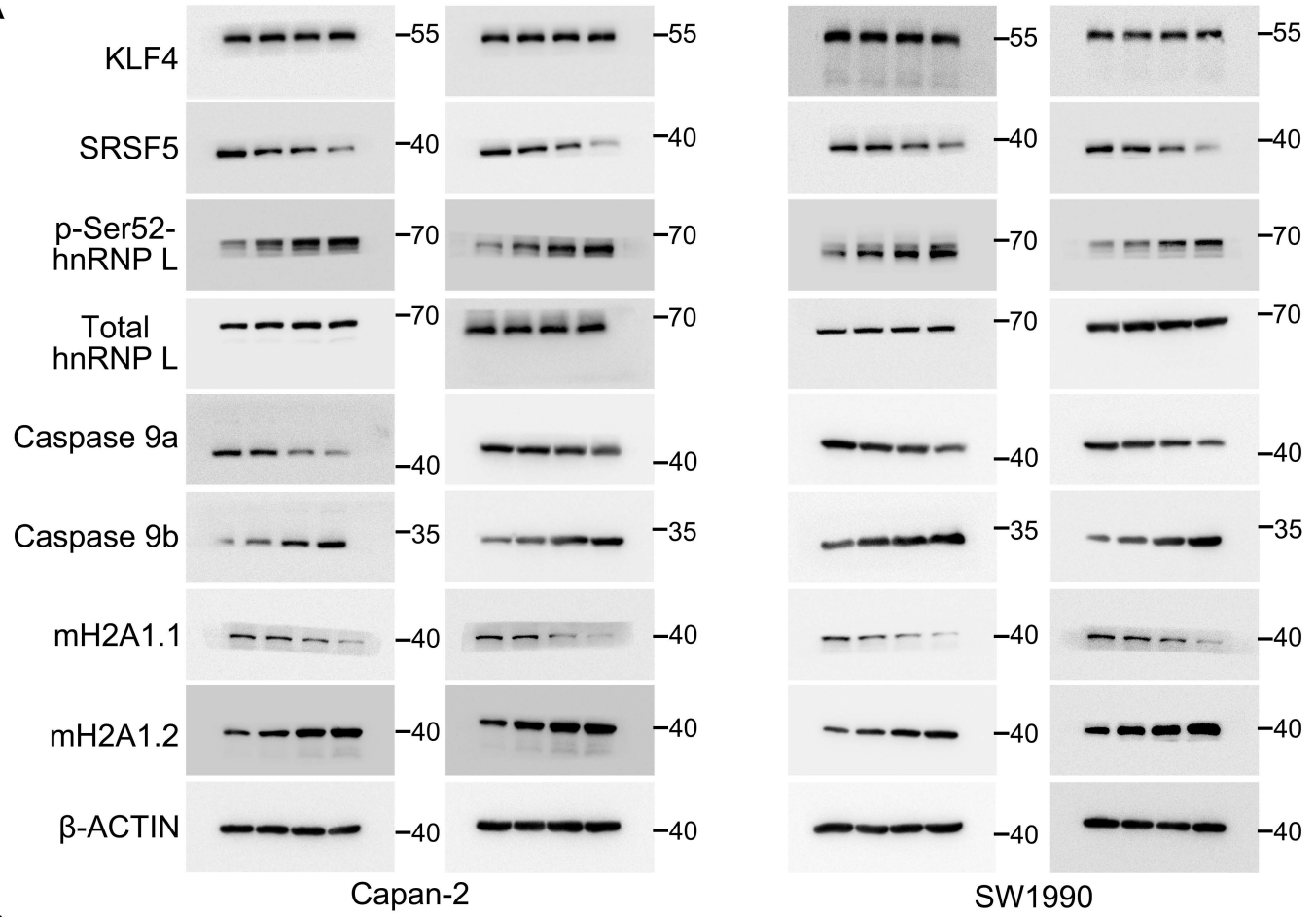

S9B

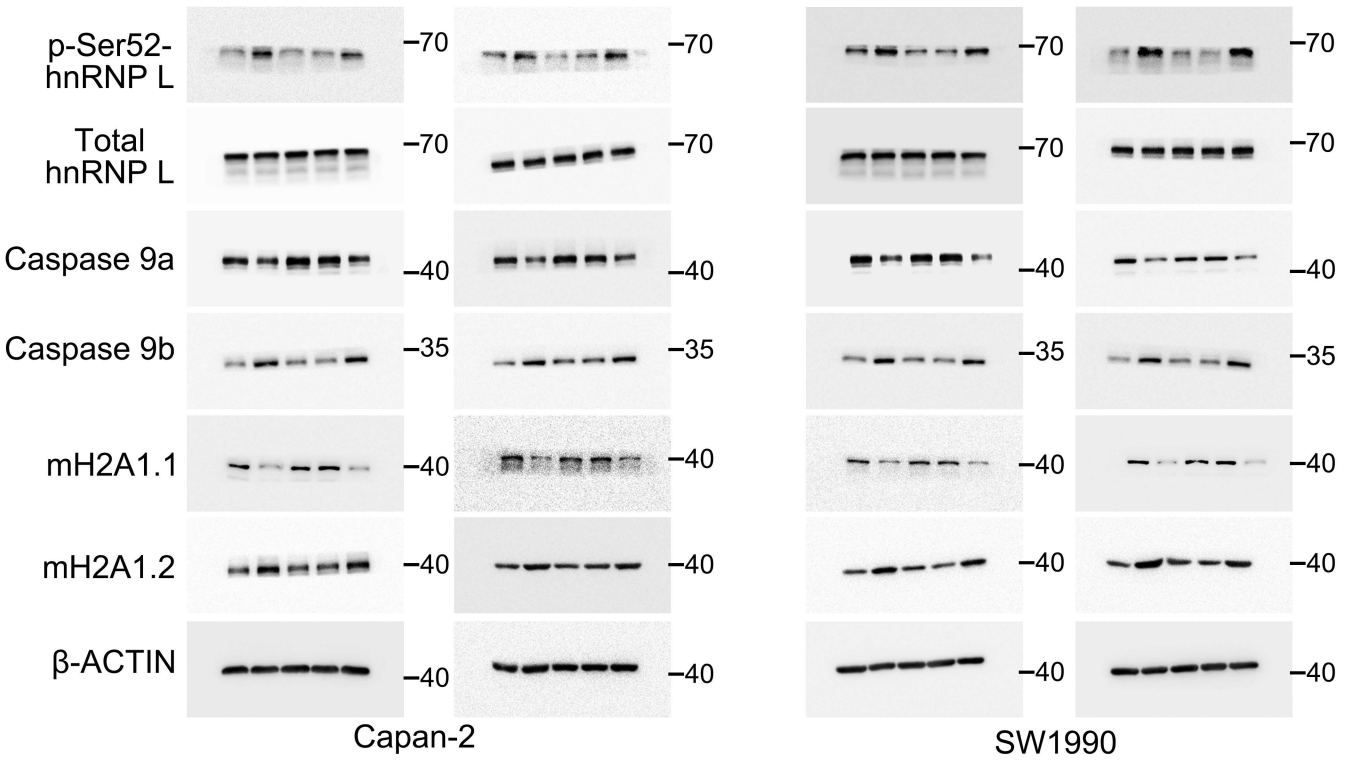

Full unedited gel for Supplementary Figure 10

S10E

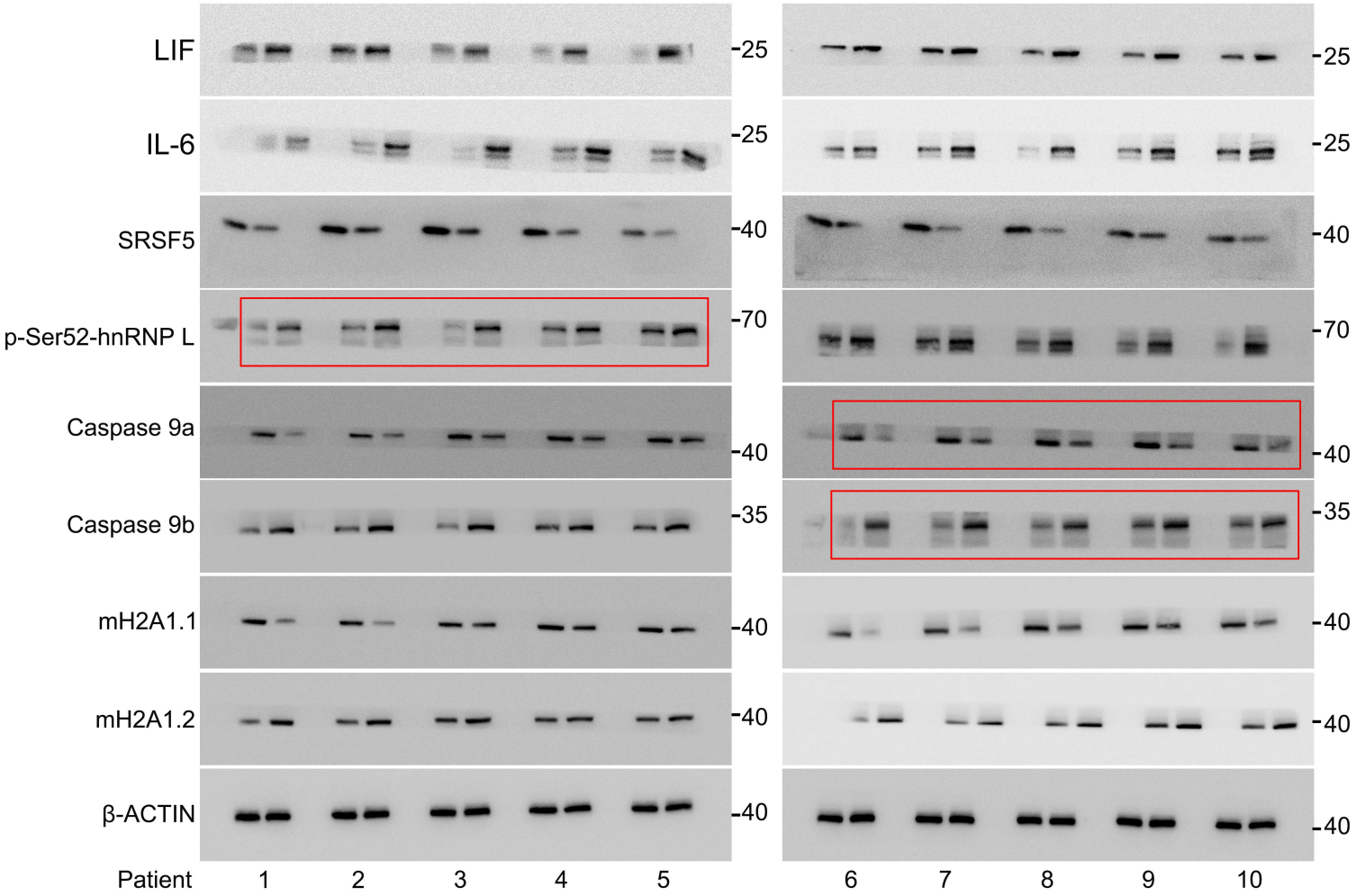

Full unedited gel for Supplementary Figure 14